Title:

Microglia replacement by ER-Hoxb8 conditionally immortalized macrophages provides insight into Aicardi-Goutières Syndrome neuropathology

Authors:

Kelsey M. Nemec[1,2], Genevieve Uy[1,3], V. Sai Chaluvadi[1,2], Freddy S. Purnell[4,5], Bilal Elfayoumi[1], Leila Byerly[6], Micaela L. O'Reilly[3], Carleigh A. O'Brien[1], William H. Aisenberg[1], Sonia I. Lombroso[1,7], Xinfeng Guo[8], Niklas Blank[9,10], Chet Huan Oon[1], Fazeela Yaqoob[1], Brian Temsamrit[3], Priyanka Rawat[3], Christoph A. Thaiss[9], Will Bailis[11,12] Adam P. Williamson[6], Qingde Wang[8], Mariko L. Bennett*[3,13], F. Chris Bennett*[1,3]

[1]Department of Psychiatry, Perelman School of Medicine, University of Pennsylvania, Philadelphia, PA, USA; [2]Department of Neuroscience, Perelman School of Medicine, University of Pennsylvania, Philadelphia, PA, USA; [3]Division of Neurology, Children's Hospital of Philadelphia, Philadelphia, PA, USA; [4]Department of Biology, School of Arts and Sciences, University of Pennsylvania, Philadelphia, PA, USA; [5]Epigenetics Institute, University of Pennsylvania, Perelman School of Medicine. Philadelphia, PA, USA; [6]Department of Biology, Bryn Mawr College, Bryn Mawr, PA, USA; [7]Department of Systems Pharmacology and Translational Therapeutics, University of Pennsylvania, Philadelphia, PA, USA; [8]Department of Surgery, University of Pittsburgh School of Medicine, Pittsburgh, PA, USA; [9]Department of Microbiology, Perelman School of Medicine, University of Pennsylvania, Philadelphia, PA, USA; [10]Faculty of Biology, University of Freiburg, Freiburg, Germany; [11]Department of Pathology and Laboratory Medicine, Children's Hospital of Philadelphia, Philadelphia, PA, USA; [12]Department of Pathology and Laboratory Medicine, Perelman School of Medicine, University of Pennsylvania, Philadelphia, PA, USA; [13]Department of Neurology, Perelman School of Medicine, University of Pennsylvania, Philadelphia, PA, USA

*Senior Authors

Acknowledgements & Funding:

We thank Dr. Richard Stanley (Albert Einstein College of Medicine, New York, NY, USA) for the Csf1r$^{-/-}$ (FVB.129X1-Csf1rtm1Ers) and Csf1r+/+ littermate animals on the FVB background; Dr. Qingde Wang (University of Pittsburgh, Pittsburgh, PA, USA) for the *Adar1* D1113H mice (p.Asp1113His); Dr. David Sykes (Mass General Hospital, Boston, MA, USA) and Dr. Igor Brodsky (University of Pennsylvania, Philadelphia, PA, USA) for the MSCVneo-HA-ER-HoxB8 plasmid; Dr. Dan Beiting for the bulk RNA sequencing DIY Transcriptomics scripts; the Children's Hospital of Philadelphia Center for Applied

Genomics for bulk RNA sequencing assistance; the Children's Hospital of Philadelphia Flow Cytometry core for flow cytometry and sorting assistance; BioRender.com for graphics; and Kayla Peelman (Emory University, Atlanta, GA, USA) for assistance with Illustrator. This work was supported by National Science Foundation Graduate Research Fellowship Program DGE-1845298 (KMN, SIL); NIH Training in Age Related Neurodegenerative Diseases T32 2-T32-AG-000255-26 (VSC); NIH Medical Scientist Training Program T32 GM007170 (VSC); NIH T32MH019112 (WHA); NIH T32 GM008076 (SIL); Blavatnik Family Fellowship, Blavatnik Foundation (SIL); NIH R35GM138085 (WB); Paul Allen Institute Distinguished Investigator Award (WB); NIH R15NS133939 (APW); R01AI139544 (QW); R01NS134651 (QW); NIH DP5OD036159 (MLB); NIH R01-NS-120960-01 (FCB); Klingenstein-Simons Fellowship in Neuroscience (FCB); and The Paul Allen Frontiers Group GRT-00000774 (FCB).

Abstract:

Microglia, the brain's resident macrophages, can be reconstituted by surrogate cells - a process termed "microglia replacement." To expand the microglia replacement toolkit, we here introduce estrogen-regulated (ER) homeobox B8 (Hoxb8) conditionally immortalized macrophages, a cell model for generation of immune cells from murine bone marrow, as a versatile model for microglia replacement. We find that ER-Hoxb8 macrophages are highly comparable to primary bone marrow-derived (BMD) macrophages in vitro, and, when transplanted into a microglia-free brain, engraft the parenchyma and differentiate into microglia-like cells. Furthermore, ER-Hoxb8 progenitors are readily transducible by virus and easily stored as stable, genetically manipulated cell lines. As a demonstration of this system's power for studying the effects of disease mutations on microglia in vivo, we created stable, *Adar1*-mutated ER-Hoxb8 lines using CRISPR-Cas9 to study the intrinsic contribution of macrophages to Aicardi-Goutières Syndrome (AGS), an inherited interferonopathy that primarily affects the brain and immune system. We find that *Adar1* knockout elicited interferon secretion and impaired macrophage production in vitro, while preventing brain macrophage engraftment in vivo - phenotypes that can be rescued with concurrent mutation of *Ifih1* (MDA5) in vitro, but not in vivo. Lastly, we extended these findings by generating ER-Hoxb8 progenitors from mice harboring a patient-specific *Adar1* mutation (D1113H). We demonstrated the ability of microglia-specific D1113H mutation to drive interferon production in vivo, suggesting microglia drive AGS neuropathology. In sum, we introduce the ER-Hoxb8 approach to model microglia replacement and use it to clarify macrophage contributions to AGS.

Keywords:
microglia; microglia replacement; ER-Hoxb8; macrophage; Aicardi-Goutières Syndrome

Introduction:
Microglia, the parenchymal tissue-resident macrophages of the brain and spinal cord, play critical roles in development, homeostasis, injury, and disease (Salter and Stevens, 2017; Li and Barres, 2018). When depleted of endogenous microglia, the brain parenchyma can be reconstituted by surrogate macrophages - a process termed "microglia replacement." Microglia replacement has the potential for precise and personalized delivery of therapeutic payloads or correction of dysfunction. Primary microglia are challenging to manipulate - they rapidly lose transcriptional identity ex vivo, resist viral manipulation, are minimally proliferative, and are highly sensitive to serum (Balcaitis et al., 2005; Jiang et al., 2012; Masuda et al., 2013; Su et al., 2016, Bohlen et al., 2017). These challenges limit the study of microglia replacement, underscoring the need for new, transplantable cell models. Common microglia surrogate cells include myeloid cells from the blood or bone marrow and induced pluripotent stem cell (iPSC)-derived microglia (iMG; Muffat et al., 2016; Pandya et al., 2017; Haenseler et al., 2017; Douvaras et al., 2017; Abud et al., 2017; Takata et al., 2020). Although capable of reconstituting the microglial niche (Priller et al., 2001; Bohlen et al., 2017; Bennett et al., 2018; Hasselmann et al., 2019), primary cells and iPSCs each have limitations that motivated us to consider new microglia replacement tools.

To create an alternative microglia surrogate, we turned to the estrogen-regulated (ER) homeobox B8 (Hoxb8) system, a method for generating and gene-editing unlimited quantities of macrophages from primary murine bone marrow (Wang et al., 2006). When overexpressed, *Hoxb8* promotes the expansion of hematopoietic progenitor cells while preventing their differentiation. When transduced with ER-Hoxb8 virus, myeloid progenitor cells from murine bone marrow become immortalized and indefinitely expandable when in the presence of exogenous estrogen, but differentiate upon estrogen removal. The ER-Hoxb8 approach has been used to generate so-called "conditionally immortalized" progenitors with lymphoid and myeloid potential (Wang et al., 2006; Rosas et al., 2011; Redecke et al., 2013; Gurzeler et al., 2013; Zach et al., 2015; Fites et al., 2018; Ma et al., 2020; Lail et al., 2022), including macrophages.

We recently showed that ER-Hoxb8 cells can reconstitute the microglial niche (Chadarevian, Lombroso, et al., 2023), supporting their potential as a new cell model for microglia replacement. Here, we aimed to deeply characterize the identity, function, and application of ER-Hoxb8s as microglia surrogates to test hypotheses about microglia-specific gene functions in health and disease.

Results:

Comparison of ER-Hoxb8 to bone marrow-derived macrophages in vitro

To directly compare primary bone marrow-derived (BMD) and ER-Hoxb8 cells, we created three biologically independent lines of conditionally immortalized macrophage progenitors as described previously (Wang et al., 2006). ER-Hoxb8 progenitor cells were plated, differentiated for seven days in CSF1, and compared to BMD macrophages (Stanley and Heard 1977; Murray et al., 2014; Figure 1A). We found that ER-Hoxb8 macrophages were highly similar to BMD macrophages morphologically (Figure 1B) and by CD11B/CD45 expression (Figure 1C, Supplemental Figures 1A/B). To validate ER-Hoxb8 macrophage function, we tested their phagocytic capacity. In agreement with prior literature (Elhag et al., 2021), ER-Hoxb8 macrophages more efficiently engulfed beads coated with 10% phosphatidlyserine (PS) to mimic apoptotic cells, compared to beads coated with phosphatidylcholine (PC) alone (Supplemental Figure 1C/D).

To expand upon previous studies (Redecke et al., 2013; Roberts et al., 2019; Accarias et al., 2020), we performed RNA sequencing of both cell types before and after seven days of differentiation. We generated high-quality transcriptomes (Phred Score > 35, n = 3 biological replicates) for BM progenitors, BM monocytes, seven-day differentiated BMD macrophages, ER-Hoxb8 progenitors, four-day differentiated ER-Hoxb8 cells, and seven-day differentiated ER-Hoxb8 macrophages (top 100 expressed genes in Supplemental Table 1). In agreement with previous literature (Wang et al., 2006), ER-Hoxb8 progenitors express canonical macrophage genes (Supplemental Figure 1E) and, interestingly, ER-Hoxb8 cells at all time points were more similar to BMD macrophages than to BM progenitors or monocytes (Supplemental Figure 1F).

Transcriptionally, seven-day differentiated ER-Hoxb8 macrophages were highly similar to BMD macrophages as demonstrated by expression of macrophage-specific genes and lack of expression of common progenitor, lymphocyte, neutrophil, and natural killer cell-specific genes (Figure 1D). Linear regression analysis between the two cell types (Figure 1E), revealed a strong correlation (R^2 = 0.96) between expression levels of all 29,625 expressed genes. We identified 85 genes as differentially expressed between ER-Hoxb8 and BMD macrophages (FDR < 0.05, Log2 Fold Change >= 2, counts per million (CPM) > 1; Figure 1F). Of these, 74 were upregulated in BMD macrophages, 11 were upregulated in ER-Hoxb8 macrophages, and no statistically significant Gene Ontology (GO) terms were found for either group (top ten DEGs by Log2FC in Supplemental Figure 1G, all DEGs in Supplemental Table 2). These data demonstrate that ER-Hoxb8 macrophages are highly similar to primary BMD macrophages in vitro.

ER-Hoxb8 cells engraft the brain parenchyma after intracranial transplantation and attain a microglia-like identity

To extend the utility of the ER-Hoxb8 model, we next studied their engraftment and identity following intracranial transplantation into *Csf1r*$^{-/-}$ hosts, which lack microglia and readily permit donor cell engraftment (Bennett et al., 2018; Figure 2A). Using BMD cells as a primary cell control, early postnatal transplantation at days zero to five (P0-5) led to robust and comparable parenchymal engraftment by 16 days (Figure 2B-D). ER-Hoxb8 macrophages engrafted at equivalent densities (171.7 cells/mm^2 +/- 8.0) as endogenous, wild-type (WT) microglia (160.0 cells/mm^2 +/- 5.5), while BMD macrophages engrafted at higher densities (264.6 cells/mm^2 +/- 6.9; Figure 2E).

BMD macrophages become "microglia-like" after engraftment in the *Csf1r*$^{-/-}$ brain (Bennett et al., 2018). Like BMD cells, ER-Hoxb8 cells lack expression of the microglia signature protein TMEM119 in vitro (Supplemental Figure 2A). After brain engraftment, we found comparably high levels of TMEM119 in BMD and ER-Hoxb8 macrophages by flow cytometry, though both had lower TMEM119 expression than endogenous microglia, consistent with prior studies (Bennett et al., 2018; Cronk et al., 2018; Shemer et al., 2018; Figure 3A). As with WT microglia and BMD macrophages, ER-Hoxb8 macrophages likewise express P2RY12 after brain engraftment (Supplemental Figure 2B)

To more comprehensively assess microglial identity, we generated high-quality bulk RNA sequencing transcriptomes (Phred Score > 35; n = 6-9 biological replicates, Supplemental Figure 2C) from isolated brain-engrafted BMD macrophages, ER-Hoxb8 macrophages, and endogenous microglia from age-matched WT hosts. Principal component analysis (PCA) and unsupervised hierarchical clustering revealed that brain residence induces both BMD and ER-Hoxb8 macrophages to become more similar to endogenous microglia (Figure 3B, Supplemental Figure 2D). We saw no evidence for batch effects between harvest days, cell sorter used, or host mouse sex (Supplemental Figure 2E). BMD and ER-Hoxb8 microglia-like cells (MLCs) were transcriptionally similar, by both PCA and linear regression analysis (Figures 3B/C/D). ER-Hoxb8 MLCs upregulated expression of canonical microglia signature genes akin to BMD controls (*P2ry12, Tmem119, Hexb, Fcrls, Gpr34, Olfml3, P2ry13, Sparc),* including genes highly downregulated in vitro (Figure 3E). Like BMD macrophages, ER-Hoxb8 macrophages lack *Sall1* expression in vivo compared to microglia (Figure 3E). Lastly, to more completely assess the degree that ER-Hoxb8 cells become "microglia-like" after brain engraftment, we compared the top up and downregulated genes from our datasets to those of brain-engrafted yolk sac (YS) progenitors using data from Bennett et al., 2018 (Supplemental Figure 2F, Supplemental Table 3). We find overlap between groups, which likewise provides a better understanding of genes that are robustly regulated by

brain engraftment. Taken together, these data show that, similar to BMD macrophages, ER-Hoxb8 macrophages become “microglia-like” with exposure to signals in the brain microenvironment.

Despite their similarities, BMD MLCs and ER-Hoxb8 MLCs have 650 differentially expressed genes (FDR < 0.05, Log2FC >= 2, and CPM > 1 in at least six of the samples (the “n” of each group); Supplemental Table 4). We performed statistical overrepresentation tests to identify relevant GO terms (Supplemental Table 5). Of particular interest were terms relating to biological processes as they concerned immune activity and reactivity. We discovered that the 34 overrepresented genes for these GO terms (Supplemental Table 6), were unique to ER-Hoxb8 MLCs, suggesting that the brain environment differentially affects engrafted BMD and ER-Hoxb8 cells, and that ER-Hoxb8 MLCs may be more primed to activation.

To gauge how significantly these transcriptomic increases in inflammation-associated genes impact the brain environment, we stained for GFAP, a marker of reactive astrocytosis and a sensitive marker for central nervous system (CNS) perturbations. We found no increase in GFAP expression across brain regions between any groups, including in brains engrafted with ER-Hoxb8 cells compared to BMD cells (Supplemental Figure 2G).

<u>*Adar1* mutation reduces macrophage number and induces interferon responses, effects mitigated by JAK inhibition or *Ifih1* mutation</u>

Having established ER-Hoxb8 macrophages as microglia-like cells, we explored their potential for study of microglia in health and disease. Building on prior work (Gran et al., 2018; Roberts et al., 2019; Accarias et al., 2021; Bromberger et al., 2022; Shen et al., 2022; Xu et al., 2022; Möller et al., 2023), we used CRISPR-Cas9 to knockout (KO) *Tlr4* in Cas9$^{+/-}$ ER-Hoxb8 progenitors, using fluorescence-activated cell sorting (FACS) to establish lines of guide-transduced ER-Hoxb8 progenitors (Supplemental Figure 3A). We confirmed editing by TIDE analysis (Supplemental Figure 3B, Brinkman et al., 2014) and protein loss by flow cytometry (Supplemental Figures 3C/D). We then verified phenotypic knockout by treating unmodified, non-targeting control (NTC) guide-transduced, and *Tlr4* guide-transduced ER-Hoxb8 macrophages with lipopolysaccharide (LPS, a *Tlr4* agonist) or R848 (a *Tlr7/8* agonist). As expected, *Tlr4* KO blunted TNF-a production in response to *Tlr4* but not *Tlr7/8* agonism (Supplemental Figure 3E).

Having validated effective gene targeting, we next leveraged strengths of the ER-Hoxb8 system to study the contribution of microglia to a monogenic CNS disease. Aicardi-Goutières Syndrome (AGS) is a rare, brain-predominant genetic

interferonopathy with nine known causal genes (Gavazzi et al., 2024). As many cells respond to interferon, it is unclear which cells drive AGS brain pathology, particularly in cases where global gene knockout is embryonic lethal. We therefore tested the hypothesis that microglia, which produce and react strongly to interferons (Zheng et al., 2015; Aw et al., 2020; Escoubas et al., 2024), are a main contributor to AGS pathology. We first confirmed that the seven coding AGS-causal genes are expressed by ER-Hoxb8 cells at similar levels to those of BMD cells and true microglia (Supplemental Figure 4A). We were primarily interested in *Adar1*, an RNA editing enzyme expressed by all brain cells, including microglia (Zhang, Chen, Sloan, et al., 2014; Bennett et al., 2016). As ADAR1 loss disrupts hematopoiesis (Wang et al., 2004; Hartner 2004), hematopoietic progenitor differentiation (XuFeng et al., 2009), and is embryonically lethal in mice (Wang et al., 2004; Hartner et al., 2004), the impact of ADAR1 loss in macrophages is unknown. We leveraged the ER-Hoxb8 model to study *Adar1* loss in macrophages by creating independent *Adar1* KO lines using two distinct sgRNAs targeting different exons (Figure 4A, Supplemental Figure 4B).

We first explored differences during differentiation of *Adar1* KO ER-Hoxb8 cells in vitro. Despite normal numbers at three days, there were significantly fewer *Adar1* KO cells during the later stages of differentiation as compared to NTC cells (Figures 4B/C, Supplemental Figures 4C/D). This suggests that either *Adar1* KO inhibits progenitor differentiation or macrophage proliferation and survival. We next performed RNA sequencing of *Adar1* KO progenitors and differentiated macrophages. *Adar1* KO progenitors were highly similar to NTC control progenitors (Figure 4D/E/F; all DEGs in Supplemental Table 7), and *Adar1* KO macrophages expressed comparable levels of macrophage-identity genes to NTC (Figure 4G), suggesting that *Adar1* KO ER-Hoxb8 progenitors can generate macrophages. At the macrophage stage, however, we found 547 DEGs (Figure 4D/E/F; Supplemental Table 8), remarkable for interferon-stimulated gene (ISG) upregulation and GO term enrichment for responses to virus, stress, cytokine stimulation, and innate immunity (Figure 4E/F; Supplemental Figure 4E, Supplemental Table 9).

To test whether *Adar1* KO-mediated interferon production underlies this macrophage phenotype, we used the Janus kinase (JAK) inhibitor Baricitinib to inhibit interferon signaling. Baricitinib, a treatment for AGS (Vanderver et al., 2020; Han et al., 2022; Kanazawa et al., 2023), caused a dose-dependent reduction in ISG expression (Figure 4H) and normalized cell counts during macrophage differentiation (Figure 4I, Supplemental Figure 4F). We validated increased type I-specific interferon (IFN-b) and ISG (CXCL10, IL6, CCL5) production by *Adar1* KO ER-Hoxb8 macrophages, and their suppression by baricitinib treatment using multiplex bead array (Figure 4J). As interferons inhibit hematopoiesis and differentiation (Demerdash et al., 2021), we

confirmed that the baricitinib-treated cells were indeed macrophages (Figure 4G) and that the ISG reduction improved macrophage production.

Melanoma differentiation associated protein 5 (MDA5, or *Ifih1)* is an epistatic modifier of *Adar1* such that deletion rescues some *Adar1* phenotypes (Liddicoat et al., 2015; Guo et al., 2022). We introduced a guide targeting *Ifih1* (BFP+) to *Adar1* KO cells (GFP+). We created single cell clones and validated double KO (dKO, GFP/BFP+) by TIDE analysis (Supplemental Figure 4H). *Ifih1* loss completely rescued the *Adar1* KO cell growth deficit during differentiation (Figure 4K), and normalized production of IFN-b, IL-6, and CCL5 (Figure 4L), but not CXCL10. As with baricitinib treatment (Supplemental Figure 4G), we found that multiple chemokines/cytokines are downregulated in *Adar1*-mutant cells as compared to NTC (TNF-a, IL-17, MIP-1a, MIP-1B, MIP-2, M-CSF), and are partially rescued by *Ifih1* deletion (Supplemental Figure 4I).

Together, these data show that *Adar1* deletion impairs macrophage but not progenitor health and is associated with interferonopathy, demonstrating the utility of the ER-HoxB8 model system for experimental isolation and study of macrophage dysfunction in a genetic disease.

<u>*Adar1* mutation prevents ER-Hoxb8 engraftment</u>

We next attempted to study how Adar1 KO macrophages affect the CNS. To our surprise, although TLR4 KO gene edited macrophages engrafted robustly (n = 10; Figure 5A/E), mice injected with *Adar1* KO cells died early and showed no engraftment in the brains of any transplanted mice that survived to endpoint (n = 3; Figure 5B/C).

Because blocking interferon signaling with baricitinib or *Ifih1* deletion correlated with better macrophage survival in vitro, we wondered if modifying our approach to limit interferon tone would permit *Adar1* KO cell engraftment. We first reduced the number of injected cells (n = 4) and harvested tissues earlier, between 4-8 days post-transplant (n = 8), and did not observe engraftment. We then tried to pre-treat donor cells and host mice with Baricitinib and likewise did not observe engraftment in surviving mice (n = 1; Figure 5E). Lastly, we transplanted *Adar1/Ifih1* dKO cells (n = 3), which showed partial rescue of *Adar1* KO phenotypes in vitro. Although we detected no areas of engraftment meeting the stringent criteria applied for our “percent area” quantification method, we noted diffuse patches of engrafted cells with rounded morphology and enlarged soma size, in three of three experimental replicates (Figure 5D/E, Supplemental Figure 5A), potentially consistent with a mild partial rescue of engraftment.

Csf1r$^{-/-}$ mice have severe constitutional, skeletal, and CNS abnormalities, typically succumbing by weaning age (Dai et al., 2002). To extend our findings about Adar1 KO macrophages in vivo we applied an inducible microglia depletion model using healthy *Cx3cr1*^{CreERT}; *Csf1r*$^{fl/fl}$ hosts (Bennett et al., 2018). After depleting endogenous microglia via subcutaneous tamoxifen injection at age P1 and P2, we intracerebrally transplanted cells into *Cx3cr1*^{CreERT}; *Csf1r*$^{fl/fl}$ brains (Supplemental Figure 5B). After 7-15 days in vivo, we saw engraftment of control (TLR4 KO and NTC; n = 4; Supplemental Figure 5C), but not *Adar1* KO cells (n = 5; Supplemental Figure 5D). Further mirroring the *Csf1r*$^{-/-}$ data, we saw small, diffuse patches of engrafted *Adar1/Ifih1* dKO cells, but none reached quantifiable levels of engraftment (n = 11; Supplemental Figure 5E). Lastly, we harvested transplanted *Cx3cr1*^{CreERT}; *Csf1r*$^{fl/fl}$ hosts early, at day three, and saw a diffuse pattern of non-quantifiable but parenchymally engrafted *Adar1* KO cells (n = 4; Supplemental Figure 5F). These data suggest that *Adar1* KO cells can enter the brain parenchyma but do not persist, consistent with the reduction in cell numbers observed in vitro during macrophage differentiation.

Overall, these results show that genetically modified ER-Hoxb8 cells robustly engraft in the brain parenchyma, which is prevented by *Adar1* KO, independent of interferon production.

<u>*Adar1* D1113H mutant ER-Hoxb8 macrophages drive brain ISG expression</u>

Most available mouse models of AGS are either embryonic lethal (Wang et al., 2004; Hartner et al., 2004; Liddicoat et al., 2015) or fail to produce CNS phenotypes (Morita et al., 2004; Ward et al., 2011; Hiller et al., 2012; Pereira-Lopes et al., 2013; Behrendt et al., 2013; Rehwinkel et al., 2013; Ohto et al., 2022). We recently created a viable mouse model harboring a patient-derived mutation (D1113H) in the catalytic domain of ADAR1, which displays robust brain ISG expression, astrocytosis, microgliosis, and white matter calcifications (Guo et al., 2022). Since AGS patient mutations are typically hypomorphic (rather than knockout), this more authentically models AGS (Rice et al., 2014). Given the non-engraftment of *Adar1* KO cells, we created ER-Hoxb8 cells from *Adar1* D1113H mice to explore the impact of AGS-specific mutations in microglia. Unlike *Adar1* KO cells, D1113H ER-Hoxb8s showed normal growth and expansion during in vitro differentiation (Figure 6A), despite a similarly increased production of IFN-b, ISGs, and other cytokines, including CXCL10, CXCL1, CCL5, VEGF, MIP-1a, and MIP-1b, but not IFN-g (Figure 6B).

We next characterized D1113H ER-Hoxb8 cells after transplantation into the *Cx3cr1*^{CreERT}; *Csf1r*$^{fl/fl}$ brain. As D1113H cells are not genetically tagged, we performed RNA in situ hybridization (ISH), using *Cre* expression (Supplemental Figure 6A/B) to distinguish endogenous microglia (*Cre*+) from donor cells (*Cre*-). Unlike *Adar* KO cells,

D1113H mutant ER-Hoxb8s engrafted the parenchyma (Figures 6C/D, n = 5 biological replicates). Notably, both D1113H homozygous mutant brains (Figure 6C) and mice engrafted with D1113H ER-Hoxb8 microglia-like cells exhibited similar and persistent upregulation in brain *Isg15*, with pockets of robust expression around engrafted Iba1+ MLCs, clustering around Iba1- nuclei that morphologically resemble neurons (Figure 6D, Supplemental Figure 7A). To get a clearer idea of their overall engraftment potential, we transplanted D1113H mutant ER-Hoxb8s into *Csf1r*$^{-/-}$ mice, which are unconfounded by repopulating endogenous microglia. Similar to brains transplanted with *Adar1/Ifih1* dKO cells, we found dispersed cell engraftment that did not reach quantifiable levels (Supplemental Figure 7B, n = 3 biological replicates). Consistent with results from *Cx3cr1*^{CreERT}; *Csf1r*$^{fl/fl}$ host mice, we saw upregulation in brain *Isg15* clustering around Iba1- nuclei (Supplemental Figure 7C, n = 3 biological replicates).

In sum, D1113H ER-Hoxb8 macrophages produce type I interferon and ISGs and induce *Isg15* production by neighboring cells after brain engraftment. These results demonstrate that *Adar1* mutation in microglia-like cells is sufficient to drive brain ISG production.

Discussion:

Realizing the potential of microglia replacement requires new tools for research and therapy development. Here, we show the power of estrogen-regulated (ER) homeobox B8 (Hoxb8) conditionally immortalized myeloid cells to robustly model microglia for rapid assessment of gene-targeted perturbations on their identity and function. We find that ER-Hoxb8 macrophages are similar to bone marrow-derived (BMD) macrophages both in vitro and in vivo, where they robustly engraft the microglia-deficient brain and upregulate microglial identity genes. We then use this model to demonstrate an approach to untangle macrophage contributions to a neurological disease, establishing the impact of macrophage-specific mutations to clinically relevant phenotypes both in vitro and in vivo.

Microglia are difficult to target and manipulate for preclinical study, necessitating the use of robust microglial surrogates for discovery, such as the ER-Hoxb8 system described here. Powerfully programmed by the brain environment, microglia lose their unique transcriptional identity in vitro (Bohlen et al., 2017; Gosselin et al., 2017) and are difficult to engineer (O'Brien et al., 2022). Common surrogates include macrophages from isolated bone marrow or immortalized cell lines derived from macrophages or microglia (Stanley and Heard, 1977; Raschke et al., 1978; Tsuchiya et al., 1980; Righi et al., 1989; Blasi et al., 1990; Chanput et al., 2014; Muffat et al., 2016; Timmerman et al., 2018).

BMD cells are finite in number and exist as a heterogeneous population. Cell lines such as induced pluripotent stem cell-derived microglia-like cells can be expensive to generate and time-intensive to maintain (Timmerman et al., 2018). ER-Hoxb8 cells are expandable, readily transducible, and brain-engraftable, making them a robust microglia surrogate. Building on the work of others (Roberts et al., 2019; Accarias et al., 2020; Xu et al., 2022), we demonstrated straightforward gene editing using CRISPR-Cas9, generated stable lines using standard cell culture reagents, and found that ER-Hoxb8s are transcriptionally similar to primary BMD cells in vitro and in vivo. We used these strengths (and spared months of generating transgenic mouse lines) to readily test hypotheses about *Adar1* function in microglia to demonstrate the potential of this system. We generated *Adar1* knockout (KO) ER-Hoxb8 lines, as well as ER-Hoxb8 lines derived from mice harboring *Adar1* patient mutations, to study the effect of microglia-specific *Adar1* mutation on macrophage generation and interferon production. The ease with which ER-Hoxb8 cells can be modified, sorted, clonally expanded, banked, and transplanted was critical to these discoveries and will enable further innovation for the study of central nervous system macrophages.

In the future, the ER-Hoxb8 system will enable additional study of *Adar1* and microglia in Aicardi-Goutières Syndrome (AGS). We found that both complete *Adar1* KO, as well as an RNA-editing catalytic domain mutation in microglia-like cells, leads to increased interferon responses cell-autonomously in vitro, as well as non-cell-autonomously as demonstrated by direct transplant. This effect is blocked by *Ifih1*/MDA5 deletion, which is thought to sense abnormal RNA species formed by *Adar1* mutation and rescues *Adar1*-catalytic domain point mutation phenotypes (Liddicoat et al., 2015; Guo et al., 2022). In contrast, brain engraftment is impacted by *Adar1* KO regardless of *Ifih1* genotype and not by Adar1 catalytic domain mutation, suggesting that the full KO phenotype may be independent of RNA editing and interferon production. Mitochondrial antiviral signaling (MAVS) adaptor protein rescues the embryonic lethality of *Adar1* null mice (Mannion et al., 2014), suggesting that manipulation of other *Adar1* pathway components could reveal *Adar1*'s role in brain engraftment and macrophage maintenance. This system can allow for interrogation of alternative *Adar1* functions, as well as other AGS mutations, and enables testing of AGS-targeted therapies.

All cell models have limitations, and we highlight two of particular relevance to the study of microglia. First, like primary BMD macrophages, ER-Hoxb8 macrophages derive from definitive as opposed to primitive hematopoiesis - the authentic origin of microglia. Though very similar to microglia, ER-Hoxb8s cannot attain full microglial identity, conspicuously lacking *Sall1* expression, an important transcription factor in regulating homeostatic microglia (Buttgereit et al., 2016). Second, we observe that ER-Hoxb8 macrophages express slightly higher levels of inflammation-associated genes than

primary BMD macrophages after brain engraftment. Though insufficient to elicit GFAP upregulation, a sensitive biomarker for inflammation, it remains an important consideration for experimental design. Interestingly, a recent study suggests it may be possible to address both limitations by treating yolk sac progenitors with the ER-Hoxb8 virus to generate macrophages with reduced inflammatory reactivity that may serve as more authentic microglia surrogates (Elhag et al., 2021). It also raises the exciting potential of an analogous system for study of human, patient-derived macrophages.

More broadly, the future of engineered microglia surrogates, including ER-Hoxb8 microglia-like cells, is bright. Leveraging the advantages of ER-Hoxb8 cells, one could create controllable gene editing via an inducible Cas9 or sgRNA and perform large, pooled screens in vitro and in vivo simultaneously, using progressively advanced methods for gene targeting. We envision microglia as potent neurotherapeutics (Bennett and Bennett, 2020), and toward that goal, the ER-Hoxb8 model provides an ideal milieu for the testing of therapeutic cell engineering strategies, such as payload delivery, synthetic receptors, and customizable gene circuits. Here we applied two engraftment models, utilizing both *Csf1r*$^{-/-}$ and inducible *Cx3cr1*^{CreERT}*; Csf1r*$^{fl/fl}$ host mice. Pairing the ER-Hoxb8 system with our CSF1R inhibitor-resistant receptor transplantation models will allow even more widespread adoption of these techniques (Chadarevian, Lombroso, et al., 2023). Together, the combination of accessible and modifiable microglial surrogates alongside increasingly effective transplantation models holds great potential for research and therapy development.

Materials/Methods:

Mouse Models

All animal studies were performed with approval from the Children's Hospital of Pennsylvania IACUC panel in accordance with institutional and national regulations. All animals were housed in a non-barrier facility with 12-hour light/dark cycles at 23+/-2 degrees C in ventilated cages with no more than five animals per cage. Animals were provided water and standard chow *ad libitum*. Cages and bedding were changed weekly.

Csf1r$^{-/-}$ (FVB.129x1-Csf1r^{tm1Ers}) and *Csf1r*$^{+/+}$ littermate animals on the FVB background were a generous gift from Dr. Richard Stanley (Albert Einstein College of Medicine). *Cx3cr1*^{CreERT}; *Csf1r*$^{fl/fl}$ mice were generated by intercrossing JAX 021212 and 021160 strains. *Adar D1113H* mice (p.Asp1113His) were a generous gift from Dr. Qingde Wang (University of Pittsburgh). For experiments using GFP-expressing donor cells, we backcrossed Osb-GFP (C57BL/6-Tg(CAG-EGFP)131Osb/LeySopJ (JAX 006567)) onto FVB WT mice (JAX 001800) for 22 generations. For experiments using

constitutively-expressed Cas9 donor cells, we used FVB.129(B6)-Gt(ROSA)26Sortm1.1(CAG-cas9*,-EGFP)Fezh/J mice (JAX 026558).

In Vitro Experiments

ER-Hoxb8 Conditionally Immortalized Cell Production

Immortalization of murine myeloid progenitor cells was completed as outlined in Wang et al. (2006). Briefly, bone marrow progenitors were isolated from the femurs and tibias of wildtype or Cas9-expressing FVB/NJ mice using a Percoll density separation (Cytiva, 17544501). Cells were cultured for three days in RPMI media (Invitrogen, 7240047) supplemented with 10 ng/mL IL3 (Peprotech, 213-13), IL6 (Peprotech, 216-16), and SCF (Peprotech, 250-03) before transduction with MSCVneo-HA-ER-Hoxb8 virus. Originally created by Dr. David Sykes (Massachusetts General Hospital), the MSCVneo-HA-ER-Hoxb8 plasmid was a generous gift from Dr. Igor Brodsky (University of Pennsylvania School of Veterinary Medicine). 24 hours after transduction, the cells were recovered and grown for 48 hours in RPMI media (Invitrogen, 7240047) supplemented with 1mM Na-Pyruvate (Invitrogen, 11360070), 0.0005 mM beta-estradiol (Sigma Aldrich, E2758), and 10 ng/mL GM-CSF (Peprotech, 315-03). Cells were then selected for transduction with the addition of 1mg/mL Geneticin (Thermofisher, 10131035) for 48 hours. Cells were then expanded and passaged every 48-72 hours at 25-50,000 cells/mL for two weeks, or until all non-immortalized cells were terminally differentiated or killed.

Bone Marrow Isolations

Bone marrow harvests were completed as previously described (Bennett et al., 2016). Briefly, femurs and tibias were dissected and flushed with 1x PBS to collect whole bone marrow. Red blood cells were then lysed with ACK Lysis Buffer (Quality Biological, 118-156-101). For experiments requiring bone marrow progenitors, whole bone marrow samples were subsequently enriched for lineage-negative cells using the Miltenyi Direct Lineage Cell Depletion Kit (130-110-470) via MACS Column separation with LS Columns (Miltenyi, 130-042-401). For experiments requiring bone marrow monocytes, whole bone marrow samples were subsequently enriched for monocytes using the Miltenyi Monocyte Isolation Kit (130-100-629) via MACS Column separation with LS Columns.

Macrophage Differentiation

Bone marrow-derived macrophages were differentiated in vitro by plating isolated bone marrow-derived progenitors in petri dishes at a density of five million cells per dish in differentiation media - DMEM media (ThermoFisher, 10569010), 10% FBS (VWR, 89510-186), 1% Penn/Strep (Invitrogen, 15140122), supplemented with 30 ng/mL

murine M-CSF (Peprotech, 315-02). Cells were differentiated for seven to nine days in a 37 degree C incubator with 5% CO_2, with media changes every two to three days.

ER-Hoxb8-derived macrophages were differentiated in vitro using methods adapted from Wang, et al. (2006). Briefly, ER-Hoxb8 progenitors were plated in petri dishes at a density of two million cells per dish, and then differentiated in the same media and timetable as noted above.

Phagocytosis Assay

C57BL/6 WT ER-Hoxb8 cells were differentiated for 7 days as described above. The day prior to the phagocytosis assay, cells were harvested via incubation with 3mM EDTA, resuspended in macrophage differentiation media, diluted to 25,000 cells/mL in macrophage differentiation media, and plated in separate wells of 8 Chambered Coverglass Systems (CellVis, C8-1.5H-N; 500µl cell dilution/12,500 cells per well). The phagocytosis assay was adapted from Williamson and Vale (2018) and Flannagan et al., 2014. Briefly, 10% phosphatidylserine (PS) beads were used to mimic apoptotic cell corpses and phosphatidylcholine (PC) beads were used to mimic live cells. 10% PS beads were 4.07µm diameter silica beads (Bangs Labs, SS05002) coated in a supported lipid bilayer composed of 10 mol.% 18:1 PS (DOPS – Avanti, 840035), 89.90 mol.% 16:0-18:1 PC (POPC – Avanti, 850457), 0.1 mol.% atto390 dye-labeled DOPE (Atto-Tec, AD 390-161). PC beads were 4.07µm diameter silica beads (Bangs Labs, SS05002) coated in a supported lipid bilayer composed of 99.90 mol.% 16:0-18:1 PC (POPC – Avanti, 850457), 0.1 mol.% atto390 dye-labeled DOPE (Atto-Tec AD 390-161). Beads were diluted to 500,000 beads/mL in macrophage differentiation media and added to the macrophages via media change, replacing old media with 500ul bead dilution per chamber of the 8 Chambered Coverglass Systems. Macrophages were incubated with synthetic apoptotic cell corpse mimics or synthetic live cell mimics for 60 minutes at 37 degrees C, 5% CO2. Cells were then fixed for 10 minutes at 37 degrees C, 5% CO2 in 4% paraformaldehyde (Sigma, P6148) in PBS, permeabilized for 1 minute in 0.1% TritonX-100 (Sigma, T8787) in PBS, and stained using HCS CellMask Green (Invitrogen, H32714). After staining, cells were placed under Aqua-Poly/Mount for imaging (Polysciences, 18606). Macrophages were imaged via spinning disk confocal microscopy on an inverted Nikon Ti2-E microscope fitted with a CSU-W1 spinning disk unit and Hamamatsu ORCA-FusionBT camera. Images were acquired using a 40x/0.95 NA objective in .nd2 format using Nikon Elements software and converted to ome-tif stacks for analysis in Fiji/ImageJ. Beads were considered ingested if HCS CellMask Green signal was visible fully surrounding a circular area inside the cell corresponding to the 4µm diameter of the silica beads. Experiments were replicated four times on four different days using independently prepared reagents each day. 81-100 cells were examined per replicate condition.

Viral Production and Transduction

To create retroviral supernatants, Lenti-X 293T cells (Takara Bio, 632180) were transfected using 850 ng/mL pCL-Eco (Addgene, 12371) and 850 ng/mL desired retroviral plasmid, supplemented with 5 ul/mL LipoD293 (SignaGen, 504782) in media containing DMEM (ThermoFisher, 10569010), 25mM HEPES (Invitrogen, 15630080), 10% FBS (VWR, 89510-186), and 1% Penn/Strep (Invitrogen, 15140122). Six hours post-transfection, media was replaced and viral supernatants were collected 48 and 72 hours later. Viral collections were combined and concentrated 10x using Retroviral Precipitation Solution (Alstem, VC200) according to manufacturer's instructions.

Transduction of ER-Hoxb8 progenitors was completed in 12-well plates coated with 1 ug/mL fibronectin (Sigma-Aldrich, F1141). Cells were plated at 200,000 cells/mL and desired titer volume of virus was added. Plates were then spun for 90 minutes at 1000xg. Post-spinfection, cells were gently mixed and resuspended in an additional 2-3 mL of fresh media. 24 hours post-transduction, cells were recovered and expanded at normal growing conditions (25-50,000 cells/mL at 37 degrees C, 5% CO_2).

CRISPR Editing

Target gene guide sequences were created using the Broad Institute's CRISPick website (Mouse GRCm38 reference genome, CRISPRko mechanism, SpyoCas9 enzyme, Hsu (2013) tracrRNA) and adapted to ligate into our plasmid backbone. This backbone, which was a generous gift from Dr. Will Bailis (University of Pennsylvania; Bailis et al., 2019) was adapted from the MSCV-MigR1-GFP/BFP plasmid (Addgene, 27490) to include a U6-driven gRNA scaffold for the insertion of guide sequences. The BbsI-HF restriction enzyme (NEB, R3539) was used to linearize the plasmid backbone at the gRNA scaffold site, and annealed guide oligos were ligated in. The ligated plasmids were then transformed using NEB Stable Cells (C3040), plated onto LB plates supplemented with 50ug/mL ampicillin, and grown for 24 hours at 30 degrees C. Correct insertion of guide sequences were confirmed using bacterial colony sanger sequencing via GeneWiz/Azenta, and full plasmid sequences were confirmed using Plasmidsaurus. Viral supernatants were then created as described above and Cas9-expressing ER-Hoxb8 macrophage progenitor cells were transduced as described above. Cells were then double-FACS sorted for transduction via fluorophore expression and expanded as normal. Successful editing was confirmed using TIDE as described in Brinkman et al. (2014). Briefly, gDNA was collected from both control and experimental macrophages and the cut site was amplified via PCR and sent for Sanger sequencing. Indel creation was then confirmed via the TIDE application (Brinkman et al., 2014; http://shinyapps.datacurators.nl/tide/). When an antibody was commercially available,

such as with TLR4 (Biolegend, 145403, PE), loss of protein was also confirmed via flow cytometry.

TNF-a ELISA

ER-Hoxb8 progenitor cells were plated and differentiated as described in the above "Macrophage Differentiation" methodology. After seven days in vitro, cells were gently removed from the petri dishes using ice cold 1x PBS + 2mM EDTA (ThermoFisher, 15575020). Cells were then re-plated at 50,000 cells/well in a TC-treated 96-well plate in 100ul fresh differentiation media. 24 hours later, LPS (Sigma, L2880-25MG) and R848 (Invivogen, TLRL-R848) were added at 100 ng/mL to respective wells. After 9.5h, supernatants were collected and diluted to 25% initial concentration to stay within kit ranges. TNF-a concentrations were measured using the TNF alpha Mouse Uncoated ELISA Kit with Plates (ThermoFisher, 88-7324-22) according to manufacturer's instructions.

***Adar1* Immunofluorescence**

ER-Hoxb8 progenitor cells were plated and differentiated as described in the above "Macrophage Differentiation" methodology. NTC and *Adar1*-edited cells were plated at 5,000 cells per well in a glass-bottom 96-well plate. Cells were fixed on day eight of differentiation in 4% PFA ((EMS, 15714) for 10 minutes. Cells were washed, blocked in 0.1% Tween20 (Bio-Rad, 1706531) + 5% donkey serum (Sigma, S39-100ML) for one hour, and then stained overnight with CD11B (BioLegend, 101208) and Hoescht 33342 Solution (ThermoFisher, 66249) at 4 degrees C. The following morning, cells were washed and imaged at 40x magnification Z-stacks using a BZ-X800 (Keyence) microscope.

***Adar1* Cell Quantification**

ER-Hoxb8 progenitor cells were plated and differentiated as described in the above "Macrophage Differentiation" methodology. NTC and *Adar1*-edited cells were plated at 5,000 cells per well in glass-bottom 96-well plates (n = 3 independently differentiated replicates per condition). Cells were plated in fresh differentiation media supplemented with nothing, vehicle (DMSO), or 10uM Baricitinib (Selleck Chemicals, S2851). Cells were plated with 125uL media on day 0, 62.5uL media was added on day 3, media was removed and replaced with 100uL media on day 6. On differentiation days 0, 3, 6, and 9, corresponding subsets of cells were stained with 1:10000 Hoescht for 30 minutes at 37 degrees C and imaged with the ImageXpress Micro Confocal System. Images were taken at 10x magnification at nine sites per well, with exposure settings consistent between wells. Cell number quantification was performed using the "Count Nuclei" pipeline in the ImageXpress software. Signal thresholds were set, masks were created over the Hoescht+ signal, and nuclei were counted (3-16 pixel width). Cell counts were

averaged across the nine imaging sites and plotted as average nuclei per field per day of differentiation.

Adar1 Multiplex Arrays

ER-Hoxb8 progenitor cells were plated and differentiated as described in the above "Macrophage Differentiation" methodology. NTC and *Adar1*-edited cells (*Adar1* KO #1, *Adar1* KO #3, *Adar1*/*Ifih1* dKO) were plated at 100,000 cells per well in an untreated 24-well plate (n=4 independently differentiated replicates per condition), whereas WT and D1113H cells were plated at 25,000 cells per well in an untreated 24-well plate (n=4 independently differentiated replicates per condition). Media was changed every two days, with the baricitinib groups receiving 0uM, 0.00064uM, 0.16uM, 0.4uM, or 10uM Baricitinib (Selleck Chemicals, S2851) with each media change. On day seven of differentiation (24h post final media change), cell supernatant was collected, spun down, and immediately frozen. Multiplexing analysis was performed using the LuminexTM 200 system by Eve Technologies Corp. (Calgary, Alberta). Assays used include the Mouse Cytokine/Chemokine 44-Plex Discovery Assay® Array (MD44), the Mouse Cytokine/Chemokine 32-Plex Discovery Assay® Array (MD32), as well as the Mouse IFN-a + IFN-b Assay (MDIFNAB). For the baricitinib groups, RNA was immediately collected from adherent cells for subsequent sequencing analyses.

<u>In Vivo Experiments</u>

Neonatal Transplantation

For intracranial transplantation into *Csf1r*$^{-/-}$ mice, p0-p5 pups were injected as previously described (Bohlen et al., 2017) by hand using a pulled glass capillary tube (World Precision Instruments, 1B100F-4) in an electrode holder connected by silicon tubing to a syringe. One microliter containing a single-cell suspension (300,000 cells/ul unless otherwise noted) of donor cells in 1x PBS was slowly injected bilaterally into cortex, 1-2mm anterior and 2-3mm lateral to lambda at a depth of 0.5-1mm. Host animals were harvested 12-16 days after injection unless otherwise noted.

Microglia/MLC Isolations

Single-cell suspensions of microglia/engrafted brain macrophages were isolated as previously described (Bennett et al., 2016). Briefly, mice were anesthetized using a cocktail of ketamine (100mg/kg) plus xylazine (10mg/kg) in 1x PBS and perfused with 10mL cold PBS. Brains were dounce homogenized in 10mL cold Medium A Buffer - 10% 10x HBSS (Fisher, 14185052), 1.5% 1M HEPES (Invitrogen, 15630080), 1.67% 30% glucose (Sigma, G7021-1KG), 86.8% ddH2O supplemented with 2% DNase (Worthington, LS002007). Homogenate was filtered through a 70um strainer and pelleted. Microglia were collected following a spin with isotonic percoll - 10% 10x HBSS,

90% Percoll PLUS density gradient media (GE Healthcare, 17544501). Cells were washed with Medium A Buffer and resuspended in desired media.

In Vivo Baricitinib Treatment

Baricitinib (Selleckchem, S2851) was reconstituted in DMSO (Sigma-Aldrich, D26250) and added to a diluent of 40% PEG300 (Sigma-Aldrich, 90878), 10% Tween80 (Sigma-Aldrich, P1754), and 50% water. Mice were administered 20uL daily by intraperitoneal injection at doses of 10mg/kg, 5mg/kg, or 1mg/kg.

Staining Experiments

Immunofluorescence

Mice were perfused with 15mL 1x PBS followed by 15mL 4% PFA (EMS, 15714) and organs were then drop-fixed in 4% PFA for 16-24 hours at 4 degrees C. Organs were then cryo-protected in 30% sucrose (Neta Scientific, SIAL-S5391-25KG), embedded in OCT (Fisher, 23-730-571), cryo-sectioned at 16um, mounted on Superfrost Plus slides (Fisher, 1255015), and frozen at -80 degrees C. Slides were then thawed at 60 degrees C, rehydrated in 1x PBS, and blocked for one hour at RT in blocking buffer - 90% 1x PBS, 9.5% donkey serum (Sigma, S39-100ML), 0.5% Triton X-100 (Sigma, T8787-50ML). After blocking, slides were incubated with primary antibodies (described below) in staining buffer (98.5% 1x PBS, 1% donkey serum, 0.5% Triton X-100) overnight at 4 degrees C. In the morning, slides were washed with 1x PBS and incubated with secondary antibodies (described below) for one hour at RT in staining buffer. Slides were washed once more and coverslipped with DAPI mounting media (EMS, 17989-60) before imaging.

Antibodies used: Rabbit Anti-Iba1 (Fujifilm, 019-19741, 1:500); Mouse Anti-GFAP (Agilent, MAB360, 1:500); Donkey anti-rabbit IgG 594 (ThermoFisher, A-21207, 1:500); Donkey anti-mouse IgG 647 (ThermoFisher, A32787, 1:500)

RNA In Situ Hybridization

In situ hybridization (ISH) was performed on mounted fixed frozen tissues using the RNAscope system per the manufacturer's protocol (Advanced Cell Diagnostics). Fluorescent detection was achieved using the RNAscope Multiplex Fluorescent Detection kit V2 (cat # 323110). Samples were probed for mouse *Isg15* (cat # 559271-C2) and *Cre* (cat # 312281-C3) and visualized with TSA Vivid dyes (cat #s 7534 and 7536). Following ISH, slides were immunostained with rabbit anti-Iba1 (cat # 019-19741, Fujifilm WAKO) and detected using fluorescently labeled donkey anti-rabbit secondary antibody (A21207, Invitrogen). Slides were coverslipped and nuclei were stained with Prolong Gold Antifade Mounting Medium with DAPI (cat # P36931, Invitrogen)

Imaging Acquisition and Processing

Slides were imaged using a BZ-X800 (Keyence) microscope. Whole-organ tile images plus z-stack images were captured and stitched/compressed using Keyence Analyzer software prior to image export. All images within experiment panels were taken with equivalent exposure settings. All images were then analyzed with FIJI (https://imagej.net/Fiji), equivalently adjusting only for brightness and black values (raw images available upon request).

Engraftment renderings were created using GFP (488) or Iba1 (594) and DAPI channels of 10x stitches. Background was equivalently subtracted using the "subtract background" function before manually thresholding via the "otsu" setting. Rendered dot masks were created by analyzing particles (size = 2-144 px; circularity = 0.5-1.0) and overlaying them on the corresponding DAPI channel. The boundaries of the brains were then outlined using the "polygon selections" tool, and everything outside this boundary was cleared and excluded from the final image.

16 um tissue sections used for RNA scope were imaged using an Andor BC43 spinning disc confocal microscope (Oxford Instruments). Sections that were directly compared were acquired using the same exposure, laser power, gain, and resolution settings. Subsequently, image analysis on raw unmanipulated images was performed using Imaris software. Representative images displayed for publication were processed equally in Imaris across all conditions to best display the data. Comprehensive notes and raw images are available upon request.

Percent Area Quantifications

For each brain sample, average total engrafted area was calculated from three matched sagittal sections (200uM apart starting at the medial-most point of the tissue), each using a 4x tile-scan image collected via Keyence microscope. Calculations were made in FIJI using the Iba1 and/or GFP channel tiled images. FIJI's "polygon selections" tool and "measure" function were used to draw and calculate a total brain ROI, as well as engrafted area ROI(s). The latter were defined as regions with Iba1+ and/or GFP+ cell groups with no fewer than 50 total cells per "group" nor 50 cells/mm^2. Edge limits of engraftment areas were defined by the nucleus of the edge-most cell being no more than 200uM from nearest-neighbor cells. Percent area engrafted was then calculated by dividing total engrafted area(s) by total brain area. Olfactory bulb was omitted for consistency as it was not present in all samples.

For each brain sample, average total area of GFAP+ cells was calculated from three matched sagittal sections (250uM apart starting at the medial-most point of the tissue),

each using a 10x tile-scan image collected via Keyence microscope. Calculations were made in FIJI using the GFAP channel tiled images. Background was equivalently subtracted from all images using the “subtract background” function. Images were then converted into 8-bit format and thresholded at 40/255 with the “intermodes” setting. ROIs were manually drawn for cortex, hippocampus, midbrain, and thalamus using FIJI’s “polygon selections” tool. Percent area covered was then calculated using the “measure” function to quantify positive GFAP signal over total ROI area.

Cell Density Quantification

For each brain sample, average cortical cell density was calculated using the same three matched sagittal sections used above to calculate area of engraftment. Here, three 20x representative images were included that spanned the cortical region of engraftment. If the region of engraftment was small, fewer images were included such that no cells overlapped and were counted more than once. Cells were counted manually using FIJI’s “Cell Counter” tool and were defined as cells that were Iba1+ and/or GFP+ and directly overlaid with a DAPI+ nucleus. Cell counts per image were averaged and divided by total area per image to obtain densities at cells/mm^2.

Morphological Analysis

All morphological analyses were performed using Fiji. Individual Iba1+ cells in the cortical parenchyma were randomly selected from 10x stitched images of the brain. For all images, individual cells were converted to 8-bit and thresholded equivalently. The despeckle function was used to remove noise from each sample. Each image was then converted to a binary image that was used for further analysis. Soma size was measured by drawing a region of interest (ROI) around somas and measuring the encompassed area. Primary branches were defined as branches extending directly from the soma and were counted manually. The length of each branch was measured from the center of the cell soma using the Neuroanatomy SNT plugin (Arshadi et al., 2021). Traces were drawn to outline branch morphology, then measured using the SNT Measurements function to obtain branch lengths.

Flow Cytometry and FACS

Once isolated into single cell suspensions, cells were washed 2x in FACS Buffer - 1x PBS, 0.5% BSA (Sigma, 126609-10GM), 0.5mM EDTA (ThermoFisher, 15575020) - and blocked with FC Block - 0.2% CD16/CD32 (BD Biosciences, 553142) in FACS Buffer - for 10m at RT. Cells were then stained using antibodies (described below) for 30-60m at 4c. Cells were washed 2x more in FACS Buffer before being analyzed or sorted as described below.

Antibodies used: LIVE/DEAD fixable far red dead cell stain kit (Invitrogen, L10120, 1:1600); Anti-mouse CD45 (PE/Cyanine7, Clone 30-F11, Biolegend, 103113, 1:400); Anti-mouse/human CD11b (PerCP/Cyanine5.5, Clone M1/70, Biolegend, 101227, 1:400); Anti-mouse monoclonal TMEM119 (PE, Clone V3RT1GOsz, Invitrogen, 12-6119-82, 1:400)

For flow cytometry experiments, stained cells were analyzed on a CytoFLEX LX (6 Laser) Flow Cytometer and visualized via FlowJo (10.8.1). For sorting experiments, stained cells were sorted with a 100uM nozzle on a FACSAria Fusion, FACSJazz, Aurora, or MoFlo Astrios depending on Core availability (no effects on data were seen between FACS machines). Cells were deposited into media for cell expansion, or TRIzol LS Reagent (Fisher, 10296028) for subsequent RNA extraction.

Bulk RNA-Sequencing and Analysis

RNA Extraction & Quantification

For in vitro populations, RNA was extracted using the Qiagen RNeasy Mini Kit (74104) according to manufacturer's instructions. For suspended populations, cells were collected and spun down at 200xg for 5m, supernatant was removed, and 350ul Buffer RLT was added directly to the cell pellet. For adherent populations, supernatant was removed, plates were washed with 1x PBS, and 650ul of Buffer RLT was added directly to the dish to create cell lysates.

For in vivo populations, cells were isolated as described in the above "Microglia/MLC Isolations" methodology and FACS sorted into TRIZol LS reagent as described in the above "Flow Cytometry and FACS" methodology. Cells were briefly vortexed and 0.2 volumes of chloroform (Sigma, C2432-500ML) were added. Cells were again vortexed, incubated for 3m at RT, and then centrifuged at 12,000xg for 15m at 4c. The upper aqueous phase was then collected and 1 volume of fresh 70% EtOH was added. Cells were again vortexed and then run through the Qiagen RNeasy Micro Kit (74004) according to manufacturer's instructions. Isolated RNA was stored at -80.

When able, RNA Integrity Numbers (RINs) were calculated using an Agilent TapeStation with High Sensitivity RNA ScreenTape (5067-5579) and Sample Buffer (5067-5580) according to manufacturer's instructions. Cells with a RIN >= 7.5 were used for subsequent library preparations. For in vitro datasets, the average RIN score was 9.03. Quantification was often not possible for brain-isolated cell populations due to low yield. In this case, all samples were used for subsequent library preparations, and quality was assessed later during preparation.

Library Preparation & Sequencing

Sequencing libraries were prepared in-house using either 40ng or 8ul RNA per sample, depending on if RIN scores and concentrations were able to be calculated as discussed above, using the NEBNext Single Cell/Low Input RNA Library Prep Kit for Illumina (NEB, E6420) according to manufacturer's instructions. Quality and quantity steps were performed using an Agilent TapeStation using High Sensitivity D5000 ScreenTape (5067-5592), and High Sensitivity D5000 Reagents (5067-5593).

Bulk RNA-sequencing of completed libraries was performed by the Children's Hospital of Philadelphia's Center for Applied Genomics (CAG) Core Facility using a NovaSeq 6000 (Illumina) system with the SP Reagent Kit v1.5 (2x100bp). Data was de-multiplexed and sent to us as FastQ files via BaseSpace (Illumina).

For sequencing of NTC and *Adar1*-edited cells with varying doses of Baricitinib, cDNA libraries were sent to Novogene for sequencing using a NovaSeq 6000 (Illumina) system with the S4 Reagent Kit (2x150bp). Data was de-multiplexed and sent to us as FastQ files for manual download. Data sequenced by Novogene was never combined with data sequenced by CAG.

Sequencing Analysis

All pre-processing steps were run using Terminal. FastQ files were downloaded from BaseSpace (Illumina) and concatenated across lanes using the "cat" function. All files were processed using FastP (Chen et al., 2018; Chen, 2023) to filter reads and trim Illumina adaptors, as well as FastQC (Andrews, 2014) to assess quality. All files were determined to be of sufficient quality for subsequent downstream processing. Reads were pseudoaligned to the mouse GRCm39 cDNA transcriptome (Ensembl release 99; Schneider et al., 2017; Zerbino et al., 2018) using Kallisto (version 0.46.0; Bray et al., 2016) and run through MultiQC (Ewels et al., 2016) for a final quality check after mapping.

All post-processing steps were run using RStudio (R Core Team, 2022). Transcripts were summarized to the gene level through tximport (version 1.14.2; Soneson et al., 2015) with abundance counts calculated via TPM and then normalized using TMM via edgeR (Robinson et al., 2010; McCarthy et al., 2012; Chen et al., 2016). Hierarchical cluster dendrograms were created using the "dist" function (method = euclidean) and "hclust" function (method = complete) and were visualized with the plot function. PCA plots were created using the "prcomp" function. Differential gene expression analysis was performed using linear modeling via limma (Ritchie et al., 2015), and differentially expressed genes (DEGs) were decided by applying an FDR cutoff of 0.05, a counts per million (CPM) cutoff of +1, and a Log2(FC) cutoff of +/- 2. Linear models and R^2 values

were created using the “lm” function. All output plots were visualized with ggplot2 (Wickham, 2016).

Statistical overrepresentation tests and related GO Terms were calculated using the Panther Classification System (Version 18.0). Respective lists of DEGs were manually imported into the Gene List Analysis tab, selected for mus musculus, and run through the statistical overrepresentation test option using the PANTHER GO-Slim options for biological process, molecular function, and cellular component. Tests were run using the Fisher’s Exact option while calculating the false discovery rate. FDR was set to a threshold of 0.05, and terms were ranked via the hierarchy option.

Statistical Calculations

GraphPad Prism (Version 10.0.0) was used to perform statistical tests and generate p values with standard designations (ns = not significant or $p >= 0.05$, $*p < 0.05$, $**p < 0.01$, $***p < 0.001$, $****p < 0.0001$). All values are shown as mean +/- standard error of the mean (SEM). Details regarding replicate numbers and individual statistical test used are provided in the respective figure legends.

References:

Abud, Edsel M., Ricardo N. Ramirez, Eric S. Martinez, Luke M. Healy, Cecilia H. H. Nguyen, Sean A. Newman, Andriy V. Yeromin, et al. 2017. “iPSC-Derived Human Microglia-like Cells to Study Neurological Diseases.” *Neuron* 94 (2): 278–93.e9.

Accarias, Solene, Thibaut Sanchez, Arnaud Labrousse, Myriam Ben-Neji, Aurélien Boyance, Renaud Poincloux, Isabelle Maridonneau-Parini, and Véronique Le Cabec. 2020. “Genetic Engineering of Hoxb8-Immortalized Hematopoietic Progenitors - a Potent Tool to Study Macrophage Tissue Migration.” *Journal of Cell Science* 133 (5). https://doi.org/10.1242/jcs.236703.

Andrews, S. 2014. “FastQC a Quality-Control Tool for High-Throughput Sequence Data.” 2014. http://www.bioinformatics.babraham.ac.uk/projects/fastqc/.

Arshadi, Cameron, Ulrik Günther, Mark Eddison, Kyle I. S. Harrington, and Tiago A. Ferreira. 2021. “SNT: A Unifying Toolbox for Quantification of Neuronal Anatomy.” Nature Methods 18 (4): 374–77.

Bailis, Will, Justin A. Shyer, Jun Zhao, Juan Carlos Garcia Canaveras, Fatimah J. Al Khazal, Rihao Qu, Holly R. Steach, et al. 2019. “Distinct Modes of Mitochondrial Metabolism Uncouple T Cell Differentiation and Function.” *Nature* 571 (7765): 403–7.

Balcaitis, Stephanie, Jonathan R. Weinstein, Sheng Li, Jeffrey S. Chamberlain, and Thomas Möller. 2005. “Lentiviral Transduction of Microglial Cells.” *Glia* 50 (1): 48–55.

Behrendt, Rayk, Tina Schumann, Alexander Gerbaulet, Laura A. Nguyen, Nadja Schubert, Dimitra Alexopoulou, Ursula Berka, et al. 2013. “Mouse SAMHD1 Has Antiretroviral Activity and Suppresses a Spontaneous Cell-Intrinsic Antiviral Response.” *Cell Reports* 4 (4): 689–96.

Bennett, F. Chris, Mariko L. Bennett, Fazeela Yaqoob, Sara B. Mulinyawe, Gerald A. Grant, Melanie Hayden Gephart, Edward D. Plowey, and Ben A. Barres. 2018. “A Combination of Ontogeny and CNS Environment Establishes Microglial Identity.” *Neuron* 98 (6): 1170–83.e8.

Bennett, Mariko L., and F. Chris Bennett. 2020. “The Influence of Environment and Origin on Brain Resident Macrophages and Implications for Therapy.” *Nature Neuroscience* 23 (2): 157–66.

Bennett, Mariko L., F. Chris Bennett, Shane A. Liddelow, Bahareh Ajami, Jennifer L. Zamanian, Nathaniel B. Fernhoff, Sara B. Mulinyawe, et al. 2016. “New Tools for Studying Microglia in the Mouse and Human CNS.” *Proceedings of the National Academy of Sciences of the United States of America* 113 (12): E1738–46.

Blasi, E., R. Barluzzi, V. Bocchini, R. Mazzolla, and F. Bistoni. 1990. “Immortalization of Murine Microglial Cells by a v-Raf/v-Myc Carrying Retrovirus.” *Journal of Neuroimmunology* 27 (2-3): 229–37.

Bohlen, Christopher J., F. Chris Bennett, Andrew F. Tucker, Hannah Y. Collins, Sara B. Mulinyawe, and Ben A. Barres. 2017. “Diverse Requirements for Microglial Survival, Specification, and Function Revealed by Defined-Medium Cultures.” *Neuron* 94 (4): 759–73.e8.

Bray, Nicolas L., Harold Pimentel, Páll Melsted, and Lior Pachter. 2016. “Near-Optimal Probabilistic RNA-Seq Quantification.” *Nature Biotechnology* 34 (5): 525–27.

Brinkman, Eva K., Tao Chen, Mario Amendola, and Bas van Steensel. 2014. “Easy Quantitative Assessment of Genome Editing by Sequence Trace Decomposition.” *Nucleic Acids Research* 42 (22): e168.

Bromberger, Thomas, Sarah Klapproth, Markus Sperandio, and Markus Moser. 2022. “Humanized β2 Integrin-Expressing Hoxb8 Cells Serve as Model to Study Integrin

Activation." *Cells* 11 (9). https://doi.org/10.3390/cells11091532.

Buttgereit, Anne, Iva Lelios, Xueyang Yu, Melissa Vrohlings, Natalie R. Krakoski, Emmanuel L. Gautier, Ryuichi Nishinakamura, Burkhard Becher, and Melanie Greter. 2016. "Sall1 Is a Transcriptional Regulator Defining Microglia Identity and Function." *Nature Immunology* 17 (12): 1397–1406.

Chadarevian, Jean Paul, Sonia I. Lombroso, Graham C. Peet, Jonathan Hasselmann, Christina Tu, Dave E. Marzan, Joia Capocchi, et al. 2023. "Engineering an Inhibitor-Resistant Human CSF1R Variant for Microglia Replacement." *The Journal of Experimental Medicine* 220 (3). https://doi.org/10.1084/jem.20220857.

Chanput, Wasaporn, Jurriaan J. Mes, and Harry J. Wichers. 2014. "THP-1 Cell Line: An in Vitro Cell Model for Immune Modulation Approach." *International Immunopharmacology* 23 (1): 37–45.

Chen, Shifu. 2023. "Ultrafast One-Pass FASTQ Data Preprocessing, Quality Control, and Deduplication Using Fastp." *iMeta* 2 (2): e107.

Chen, Shifu, Yanqing Zhou, Yaru Chen, and Jia Gu. 2018. "Fastp: An Ultra-Fast All-in-One FASTQ Preprocessor." *Bioinformatics* 34 (17): i884–90.

Chen, Yunshun, Aaron T. L. Lun, and Gordon K. Smyth. 2016. "From Reads to Genes to Pathways: Differential Expression Analysis of RNA-Seq Experiments Using Rsubread and the edgeR Quasi-Likelihood Pipeline." *F1000Research* 5 (June):1438.

Cronk, James C., Anthony J. Filiano, Antoine Louveau, Ioana Marin, Rachel Marsh, Emily Ji, Dylan H. Goldman, et al. 2018. "Peripherally Derived Macrophages Can Engraft the Brain Independent of Irradiation and Maintain an Identity Distinct from Microglia." *The Journal of Experimental Medicine* 215 (6): 1627–47.

Dai, Xu-Ming, Gregory R. Ryan, Andrew J. Hapel, Melissa G. Dominguez, Robert G. Russell, Sara Kapp, Vonetta Sylvestre, and E. Richard Stanley. 2002. "Targeted Disruption of the Mouse Colony-Stimulating Factor 1 Receptor Gene Results in Osteopetrosis, Mononuclear Phagocyte Deficiency, Increased Primitive Progenitor Cell Frequencies, and Reproductive Defects." *Blood* 99 (1): 111–20.

Demerdash, Yasmin, Bailee Kain, Marieke A. G. Essers, and Katherine Y. King. 2021. "Yin and Yang: The Dual Effects of Interferons on Hematopoiesis." *Experimental Hematology* 96 (April):1–12.

Douvaras, Panagiotis, Bruce Sun, Minghui Wang, Ilya Kruglikov, Gregory Lallos, Matthew Zimmer, Cecile Terrenoire, et al. 2017. “Directed Differentiation of Human Pluripotent Stem Cells to Microglia.” *Stem Cell Reports* 8 (6): 1516–24.

Elhag, Sara, Christopher Stremmel, Annette Zehrer, Josefine Plocke, Roman Hennel, Michaela Keuper, Clarissa Knabe, et al. 2021. “Differences in Cell-Intrinsic Inflammatory Programs of Yolk Sac and Bone Marrow Macrophages.” *Cells* 10 (12). https://doi.org/10.3390/cells10123564.

Escoubas, Caroline C., Leah C. Dorman, Phi T. Nguyen, Christian Lagares-Linares, Haruna Nakajo, Sarah R. Anderson, Jerika J. Barron, et al. 2024. “Type-I-Interferon-Responsive Microglia Shape Cortical Development and Behavior.” *Cell* 187 (8): 1936–54.e24.

Ewels, Philip, Måns Magnusson, Sverker Lundin, and Max Käller. 2016. “MultiQC: Summarize Analysis Results for Multiple Tools and Samples in a Single Report.” *Bioinformatics* 32 (19): 3047–48.

Fites, J. Scott, Michael Gui, John F. Kernien, Paige Negoro, Zeina Dagher, David B. Sykes, Jeniel E. Nett, Michael K. Mansour, and Bruce S. Klein. 2018. “An Unappreciated Role for Neutrophil-DC Hybrids in Immunity to Invasive Fungal Infections.” *PLoS Pathogens* 14 (5): e1007073.

Flannagan, Ronald S., Johnathan Canton, Wendy Furuya, Michael Glogauer, and Sergio Grinstein. 2014. “The Phosphatidylserine Receptor TIM4 Utilizes Integrins as Coreceptors to Effect Phagocytosis.” Molecular Biology of the Cell 25 (9): 1511–22.

Gavazzi, Francesco, Carlos Dominguez Gonzalez, Kaley Arnold, Meghan Swantkowski, Lauren Charlton, Nicholson Modesti, Asif A. Dar, Adeline Vanderver, Mariko Bennett, and Laura A. Adang. 2024. “Nucleotide Metabolism, Leukodystrophies, and CNS Pathology.” *Journal of Inherited Metabolic Disease*, February. https://doi.org/10.1002/jimd.12721.

Gosselin, David, Dylan Skola, Nicole G. Coufal, Inge R. Holtman, Johannes C. M. Schlachetzki, Eniko Sajti, Baptiste N. Jaeger, et al. 2017. “An Environment-Dependent Transcriptional Network Specifies Human Microglia Identity.” *Science* 356 (6344). https://doi.org/10.1126/science.aal3222.

Gran, Sandra, Lisa Honold, Olesja Fehler, Stefanie Zenker, Sarah Eligehausen, Michael T. Kuhlmann, Edwin Geven, et al. 2018. “Imaging, Myeloid Precursor Immortalization,

and Genome Editing for Defining Mechanisms of Leukocyte Recruitment in Vivo." *Theranostics* 8 (9): 2407–23.

Guo, Xinfeng, Richard A. Steinman, Yi Sheng, Guodong Cao, Clayton A. Wiley, and Qingde Wang. 2022. "An AGS-Associated Mutation in ADAR1 Catalytic Domain Results in Early-Onset and MDA5-Dependent Encephalopathy with IFN Pathway Activation in the Brain." *Journal of Neuroinflammation* 19 (1): 285.

Gurzeler, U., T. Rabachini, C. A. Dahinden, M. Salmanidis, G. Brumatti, P. G. Ekert, N. Echeverry, D. Bachmann, H. U. Simon, and T. Kaufmann. 2013. "In Vitro Differentiation of near-Unlimited Numbers of Functional Mouse Basophils Using Conditional Hoxb8." *Allergy* 68 (5): 604–13.

Haenseler, Walther, Stephen N. Sansom, Julian Buchrieser, Sarah E. Newey, Craig S. Moore, Francesca J. Nicholls, Satyan Chintawar, et al. 2017. "A Highly Efficient Human Pluripotent Stem Cell Microglia Model Displays a Neuronal-Co-Culture-Specific Expression Profile and Inflammatory Response." *Stem Cell Reports* 8 (6): 1727–42.

Han, Velda X., Shekeeb S. Mohammad, Hannah F. Jones, Sushil Bandodkar, Yanick J. Crow, Russell C. Dale, and AGS-JAKi Study Group. 2022. "Cerebrospinal Fluid Neopterin as a Biomarker of Treatment Response to Janus Kinase Inhibition in Aicardi-Goutières Syndrome." *Developmental Medicine and Child Neurology* 64 (2): 266–71.

Hartner, Jochen C., Carolin Schmittwolf, Andreas Kispert, Albrecht M. Müller, Miyoko Higuchi, and Peter H. Seeburg. 2004. "Liver Disintegration in the Mouse Embryo Caused by Deficiency in the RNA-Editing Enzyme ADAR1." *The Journal of Biological Chemistry* 279 (6): 4894–4902.

Hasselmann, Jonathan, Morgan A. Coburn, Whitney England, Dario X. Figueroa Velez, Sepideh Kiani Shabestari, Christina H. Tu, Amanda McQuade, et al. 2019. "Development of a Chimeric Model to Study and Manipulate Human Microglia In Vivo." *Neuron* 103 (6): 1016–33.e10.

Hiller, Bjoern, Martin Achleitner, Silke Glage, Ronald Naumann, Rayk Behrendt, and Axel Roers. 2012. "Mammalian RNase H2 Removes Ribonucleotides from DNA to Maintain Genome Integrity." *The Journal of Experimental Medicine* 209 (8): 1419–26.

Jiang, Xiao-Shuang, Ying-Qin Ni, Tian-Jin Liu, Meng Zhang, Hui Ren, Rui Jiang, Xin Huang, and Ge-Zhi Xu. 2012. "CCR2 Overexpression Promotes the Efficient

Recruitment of Retinal Microglia in Vitro.” *Molecular Vision* 18 (December): 2982–92.

Kanazawa, Nobuo, Taeko Ishii, Yasushi Takita, Atsushi Nishikawa, and Ryuta Nishikomori. 2023. “Efficacy and Safety of Baricitinib in Japanese Patients with Autoinflammatory Type I Interferonopathies (NNS/CANDLE, SAVI, And AGS).” *Pediatric Rheumatology Online Journal* 21 (1): 38.

Li, Qingyun, and Ben A. Barres. 2018. “Microglia and Macrophages in Brain Homeostasis and Disease.” *Nature Reviews. Immunology* 18 (4): 225–42.

Liddicoat, Brian J., Robert Piskol, Alistair M. Chalk, Gokul Ramaswami, Miyoko Higuchi, Jochen C. Hartner, Jin Billy Li, Peter H. Seeburg, and Carl R. Walkley. 2015. “RNA Editing by ADAR1 Prevents MDA5 Sensing of Endogenous dsRNA as Nonself.” *Science* 349 (6252): 1115–20.

Ma, Guangxin, Deniz Gezer, Oliver Herrmann, Kristina Feldberg, Mirle Schemionek, Mohamad Jawhar, Andreas Reiter, Tim H. Brümmendorf, Steffen Koschmieder, and Nicolas Chatain. 2020. “LCP1 Triggers mTORC2/AKT Activity and Is Pharmacologically Targeted by Enzastaurin in Hypereosinophilia.” *Molecular Carcinogenesis* 59 (1): 87–103.

Mannion, Niamh M., Sam M. Greenwood, Robert Young, Sarah Cox, James Brindle, David Read, Christoffer Nellåker, et al. 2014. “The RNA-Editing Enzyme ADAR1 Controls Innate Immune Responses to RNA.” *Cell Reports* 9 (4): 1482–94.

Masuda, Takahiro, Makoto Tsuda, Hidetoshi Tozaki-Saitoh, and Kazuhide Inoue. 2013. “Lentiviral Transduction of Cultured Microglia.” *Methods in Molecular Biology* 1041:63–67.

McCarthy, Davis J., Yunshun Chen, and Gordon K. Smyth. 2012. “Differential Expression Analysis of Multifactor RNA-Seq Experiments with Respect to Biological Variation.” *Nucleic Acids Research* 40 (10): 4288–97.

Möller, Alexander, Saskia-Larissa Jauch-Speer, Shrey Gandhi, Thomas Vogl, Johannes Roth, and Olesja Fehler. 2023. “The Roles of Toll-like Receptor 4, CD33, CD68, CD69, or CD147/EMMPRIN for Monocyte Activation by the DAMP S100A8/S100A9.” *Frontiers in Immunology* 14 (March):1110185.

Morita, Masashi, Gordon Stamp, Peter Robins, Anna Dulic, Ian Rosewell, Geza Hrivnak, Graham Daly, Tomas Lindahl, and Deborah E. Barnes. 2004. “Gene-Targeted

Mice Lacking the Trex1 (DNase III) 3'-->5' DNA Exonuclease Develop Inflammatory Myocarditis." *Molecular and Cellular Biology* 24 (15): 6719–27.

Muffat, Julien, Yun Li, Bingbing Yuan, Maisam Mitalipova, Attya Omer, Sean Corcoran, Grisilda Bakiasi, et al. 2016. "Efficient Derivation of Microglia-like Cells from Human Pluripotent Stem Cells." *Nature Medicine* 22 (11): 1358–67.

Murray, Peter J., Judith E. Allen, Subhra K. Biswas, Edward A. Fisher, Derek W. Gilroy, Sergij Goerdt, Siamon Gordon, et al. 2014. "Macrophage Activation and Polarization: Nomenclature and Experimental Guidelines." *Immunity* 41 (1): 14–20.

O'Brien, Carleigh A., F. Chris Bennett, and Mariko L. Bennett. 2022. "Microglia in Antiviral Immunity of the Brain and Spinal Cord." *Seminars in Immunology* 60 (March):101650.

Ohto, Taisuke, Ahmed Abu Tayeh, Ryuta Nishikomori, Hiroto Abe, Kyota Hashimoto, Shiro Baba, Anahi-Paula Arias-Loza, et al. 2022. "Intracellular Virus Sensor MDA5 Mutation Develops Autoimmune Myocarditis and Nephritis." *Journal of Autoimmunity* 127 (February):102794.

Pandya, Hetal, Michael J. Shen, David M. Ichikawa, Andrea B. Sedlock, Yong Choi, Kory R. Johnson, Gloria Kim, et al. 2017. "Differentiation of Human and Murine Induced Pluripotent Stem Cells to Microglia-like Cells." *Nature Neuroscience* 20 (5): 753–59.

Pereira-Lopes, Selma, Teja Celhar, Gloria Sans-Fons, Maria Serra, Anna-Marie Fairhurst, Jorge Lloberas, and Antonio Celada. 2013. "The Exonuclease Trex1 Restrains Macrophage Proinflammatory Activation." *Journal of Immunology* 191 (12): 6128–35.

Priller, J., A. Flügel, T. Wehner, M. Boentert, C. A. Haas, M. Prinz, F. Fernández-Klett, et al. 2001. "Targeting Gene-Modified Hematopoietic Cells to the Central Nervous System: Use of Green Fluorescent Protein Uncovers Microglial Engraftment." *Nature Medicine* 7 (12): 1356–61.

R Core Team. 2022. "R: A Language and Environment for Statistical Computing." Foundation for Statistical Computing, Vienna, Austria. 2022. https://www.R-project.org/.

Raschke, W. C., S. Baird, P. Ralph, and I. Nakoinz. 1978. "Functional Macrophage Cell Lines Transformed by Abelson Leukemia Virus." *Cell* 15 (1): 261–67.

Redecke, Vanessa, Ruiqiong Wu, Jingran Zhou, David Finkelstein, Vandana Chaturvedi, Anthony A. High, and Hans Häcker. 2013. “Hematopoietic Progenitor Cell Lines with Myeloid and Lymphoid Potential.” *Nature Methods* 10 (8): 795–803.

Rehwinkel, Jan, Jonathan Maelfait, Anne Bridgeman, Rachel Rigby, Bruce Hayward, Rachel A. Liberatore, Paul D. Bieniasz, et al. 2013. “SAMHD1-Dependent Retroviral Control and Escape in Mice.” *The EMBO Journal* 32 (18): 2454–62.

Rice, Gillian I., Yoandris Del Toro Duany, Emma M. Jenkinson, Gabriella Ma Forte, Beverley H. Anderson, Giada Ariaudo, Brigitte Bader-Meunier, et al. 2014. “Gain-of-Function Mutations in IFIH1 Cause a Spectrum of Human Disease Phenotypes Associated with Upregulated Type I Interferon Signaling.” *Nature Genetics* 46 (5): 503–9.

Righi, M., L. Mori, G. De Libero, M. Sironi, A. Biondi, A. Mantovani, S. D. Donini, and P. Ricciardi-Castagnoli. 1989. “Monokine Production by Microglial Cell Clones.” *European Journal of Immunology* 19 (8): 1443–48.

Ritchie, Matthew E., Belinda Phipson, Di Wu, Yifang Hu, Charity W. Law, Wei Shi, and Gordon K. Smyth. 2015. “Limma Powers Differential Expression Analyses for RNA-Sequencing and Microarray Studies.” *Nucleic Acids Research* 43 (7): e47.

Roberts, Allison W., Lauren M. Popov, Gabriel Mitchell, Krystal L. Ching, Daniel J. Licht, Guillaume Golovkine, Gregory M. Barton, and Jeffery S. Cox. 2019. “Cas9+ Conditionally-Immortalized Macrophages as a Tool for Bacterial Pathogenesis and beyond.” *eLife* 8 (June):e45957.

Robinson, Mark D., Davis J. McCarthy, and Gordon K. Smyth. 2010. “edgeR: A Bioconductor Package for Differential Expression Analysis of Digital Gene Expression Data.” *Bioinformatics* 26 (1): 139–40.

Rosas, Marcela, Fabiola Osorio, Matthew J. Robinson, Luke C. Davies, Nicola Dierkes, Simon A. Jones, Caetano Reis e Sousa, and Philip R. Taylor. 2011. “Hoxb8 Conditionally Immortalised Macrophage Lines Model Inflammatory Monocytic Cells with Important Similarity to Dendritic Cells.” *European Journal of Immunology* 41 (2): 356–65.

Salter, Michael W., and Beth Stevens. 2017. “Microglia Emerge as Central Players in Brain Disease.” *Nature Medicine* 23 (9): 1018–27.

Schneider, Valerie A., Tina Graves-Lindsay, Kerstin Howe, Nathan Bouk, Hsiu-Chuan Chen, Paul A. Kitts, Terence D. Murphy, et al. 2017. “Evaluation of GRCh38 and de Novo Haploid Genome Assemblies Demonstrates the Enduring Quality of the Reference Assembly.” *Genome Research* 27 (5): 849–64.

Shemer, Anat, Jonathan Grozovski, Tuan Leng Tay, Jenhan Tao, Alon Volaski, Patrick Süß, Alberto Ardura-Fabregat, et al. 2018. “Engrafted Parenchymal Brain Macrophages Differ from Microglia in Transcriptome, Chromatin Landscape and Response to Challenge.” *Nature Communications* 9 (1): 5206.

Shen, Zeyang, Rick Z. Li, Thomas A. Prohaska, Marten A. Hoeksema, Nathan J. Spann, Jenhan Tao, Gregory J. Fonseca, et al. 2022. “Systematic Analysis of Naturally Occurring Insertions and Deletions That Alter Transcription Factor Spacing Identifies Tolerant and Sensitive Transcription Factor Pairs.” *eLife* 11 (January):e70878.

Soneson, Charlotte, Michael I. Love, and Mark D. Robinson. 2015. “Differential Analyses for RNA-Seq: Transcript-Level Estimates Improve Gene-Level Inferences.” *F1000Research* 4 (December):1521.

Stanley, E. R., and P. M. Heard. 1977. “Factors Regulating Macrophage Production and Growth. Purification and Some Properties of the Colony Stimulating Factor from Medium Conditioned by Mouse L Cells.” *The Journal of Biological Chemistry* 252 (12): 4305–12.

Su, Wei, John Kang, Bryce Sopher, James Gillespie, Macarena S. Aloi, Guy L. Odom, Stephanie Hopkins, et al. 2016. “Recombinant Adeno-Associated Viral (rAAV) Vectors Mediate Efficient Gene Transduction in Cultured Neonatal and Adult Microglia.” *Journal of Neurochemistry* 136 Suppl 1 (0 1): 49–62.

Takata, Kazuyuki, Tatsuya Kozaki, Christopher Zhe Wei Lee, Morgane Sonia Thion, Masayuki Otsuka, Shawn Lim, Kagistia Hana Utami, et al. 2020. “Induced-Pluripotent-Stem-Cell-Derived Primitive Macrophages Provide a Platform for Modeling Tissue-Resident Macrophage Differentiation and Function.” *Immunity* 52 (2): 417–18.

Timmerman, Raissa, Saskia M. Burm, and Jeffrey J. Bajramovic. 2018. “An Overview of in Vitro Methods to Study Microglia.” *Frontiers in Cellular Neuroscience* 12 (August):242.

Tsuchiya, S., M. Yamabe, Y. Yamaguchi, Y. Kobayashi, T. Konno, and K. Tada. 1980.

“Establishment and Characterization of a Human Acute Monocytic Leukemia Cell Line (THP-1).” *International Journal of Cancer. Journal International Du Cancer* 26 (2): 171–76.

Vanderver, Adeline, Laura Adang, Francesco Gavazzi, Katherine McDonald, Guy Helman, David B. Frank, Nicole Jaffe, et al. 2020. “Janus Kinase Inhibition in the Aicardi-Goutières Syndrome.” *The New England Journal of Medicine* 383 (10): 986–89.

Wang, Gang G., Katherine R. Calvo, Martina P. Pasillas, David B. Sykes, Hans Häcker, and Mark P. Kamps. 2006. “Quantitative Production of Macrophages or Neutrophils Ex Vivo Using Conditional Hoxb8.” *Nature Methods* 3 (4): 287–93.

Ward, Simone V., Cyril X. George, Megan J. Welch, Li-Ying Liou, Bumsuk Hahm, Hanna Lewicki, Juan C. de la Torre, Charles E. Samuel, and Michael B. Oldstone. 2011. “RNA Editing Enzyme Adenosine Deaminase Is a Restriction Factor for Controlling Measles Virus Replication That Also Is Required for Embryogenesis.” *Proceedings of the National Academy of Sciences* 108 (1): 331–36.

Williamson, Adam P., and Ronald D. Vale. 2018. “Spatial Control of Draper Receptor Signaling Initiates Apoptotic Cell Engulfment.” The Journal of Cell Biology 217 (11): 3977–92.

Xu, Jane Jialu, Alistair M. Chalk, Iva Nikolic, Kaylene J. Simpson, Monique F. Smeets, and Carl R. Walkley. 2022. “Genome-Wide Screening Identifies Cell-Cycle Control as a Synthetic Lethal Pathway with SRSF2P95H Mutation.” *Blood Advances* 6 (7): 2092–2106.

XuFeng, Richard, Matthew J. Boyer, Hongmei Shen, Yanxin Li, Hui Yu, Yindai Gao, Qiong Yang, Qingde Wang, and Tao Cheng. 2009. “ADAR1 Is Required for Hematopoietic Progenitor Cell Survival via RNA Editing.” *Proceedings of the National Academy of Sciences of the United States of America* 106 (42): 17763–68.

Zach, Frank, Alexandra Mueller, and André Gessner. 2015. “Production and Functional Characterization of Murine Osteoclasts Differentiated from ER-Hoxb8-Immortalized Myeloid Progenitor Cells.” *PloS One* 10 (11): e0142211.

Zerbino, Daniel R., Premanand Achuthan, Wasiu Akanni, M. Ridwan Amode, Daniel Barrell, Jyothish Bhai, Konstantinos Billis, et al. 2018. “Ensembl 2018.” *Nucleic Acids Research* 46 (D1): D754–61.

Zhang, Ye, Kenian Chen, Steven A. Sloan, Mariko L. Bennett, Anja R. Scholze, Sean O'Keeffe, Hemali P. Phatnani, et al. 2014. "An RNA-Sequencing Transcriptome and Splicing Database of Glia, Neurons, and Vascular Cells of the Cerebral Cortex." The Journal of Neuroscience: The Official Journal of the Society for Neuroscience 34 (36): 11929–47.

Zheng, Lian-Shun, Naoko Kaneko, and Kazunobu Sawamoto. 2015. "Minocycline Treatment Ameliorates Interferon-Alpha- Induced Neurogenic Defects and Depression-like Behaviors in Mice." *Frontiers in Cellular Neuroscience* 9 (January):5.

Figures:

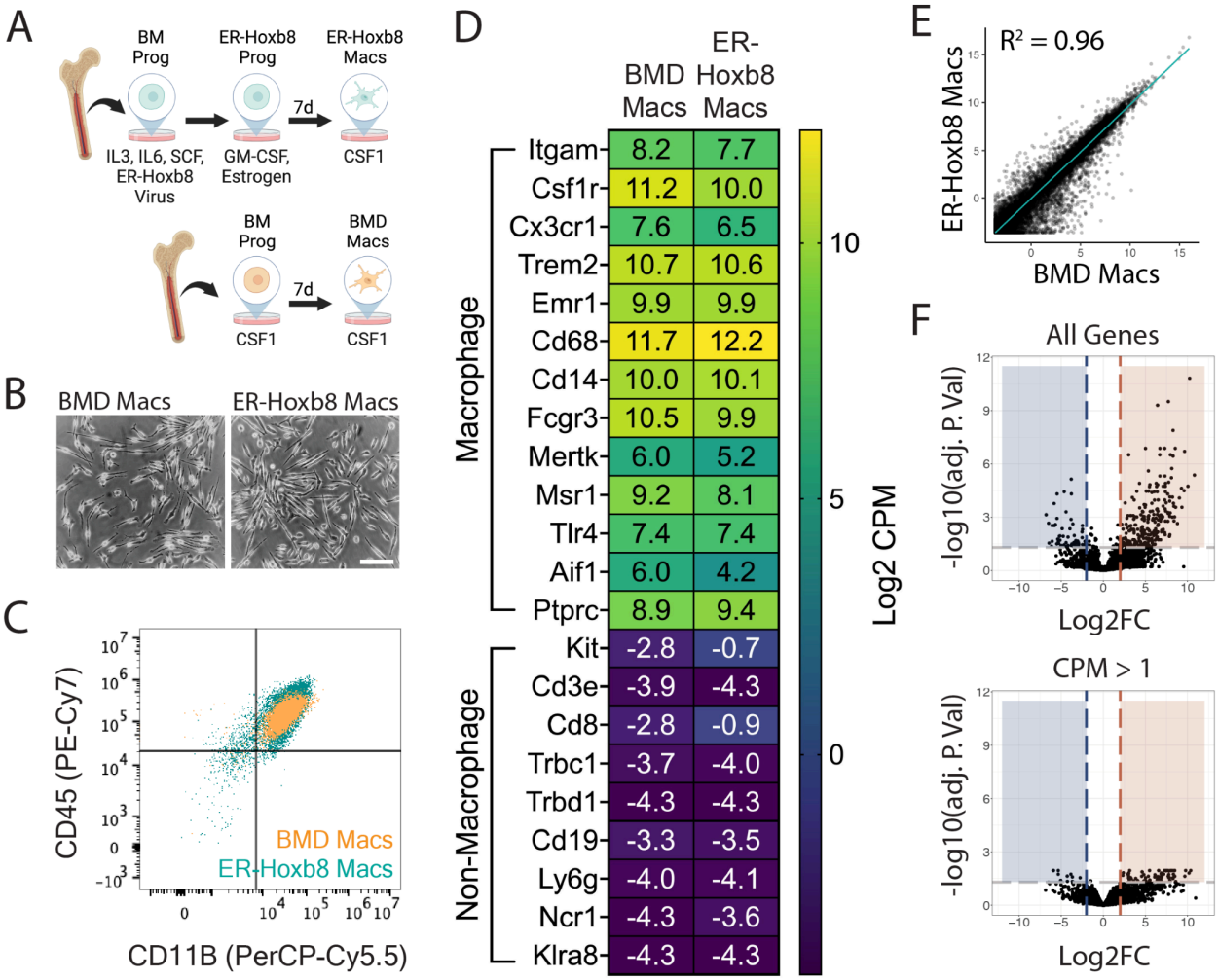

Figure 1: Comparison of ER-Hoxb8 to BMD macrophages in vitro. (A) Schematic for creation of bone marrow-derived (BMD) and ER-Hoxb8 cells **(B)** Brightfield images of BMD and ER-Hoxb8 macrophages plated in the presence of 30ng/mL mouse CSF1 and differentiated for seven days (scale bar = 100um) **(C)** Dot plot representing CD45/CD11B levels (pre-gated on live, singlet, leukocyte) by flow cytometry **(D)** Heatmap showing Log2 CPM of canonical macrophage (top) and non-macrophage (bottom) immune cell genes **(E)** Whole transcriptome comparison between BMD and ER-Hoxb8 macrophages, depicting best fit line and coefficient of determination (one dot = one gene) **(F)** Volcano plots comparing all genes or those with CPM > 1 (Log2FC >= 2, FDR < 0.05); blue = upregulated in ER-Hoxb8 macrophages, red = upregulated in BMD macrophages

Panel A created with BioRender.com/w42j197

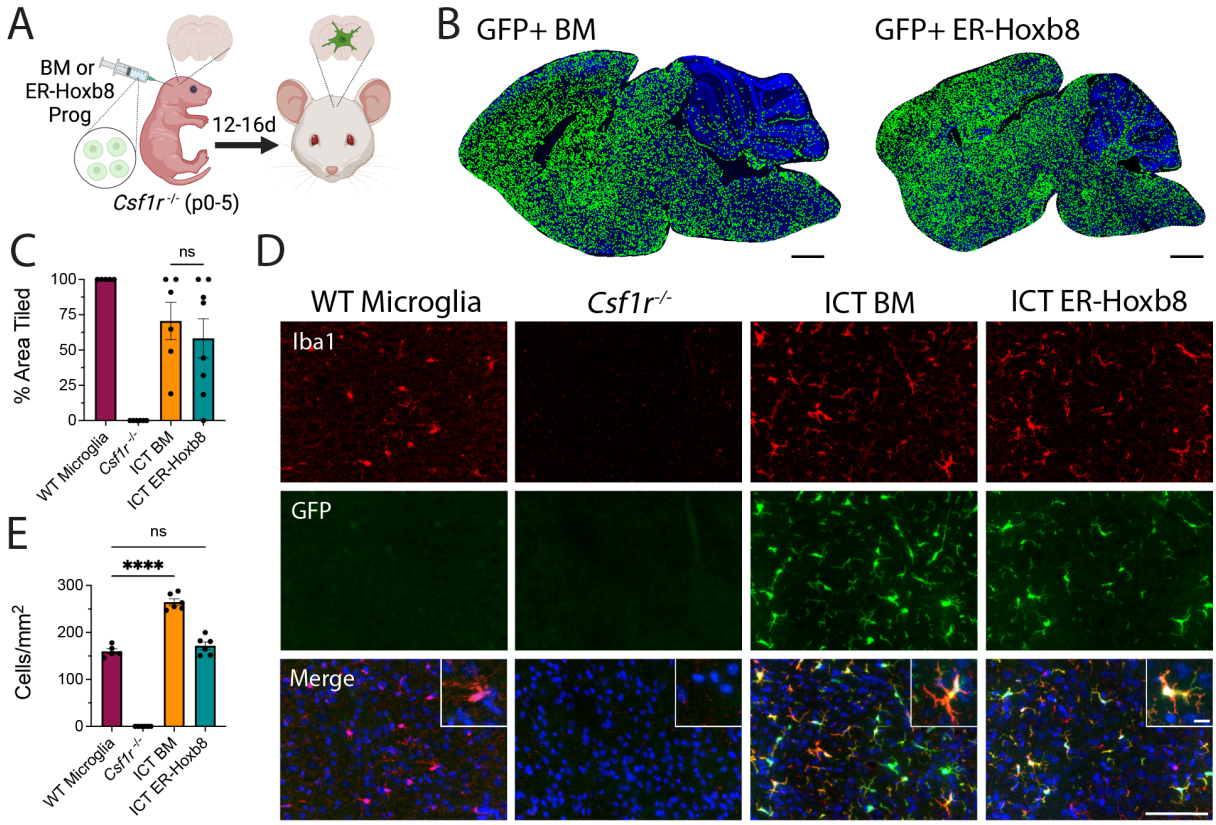

Figure 2: Engraftment potential of ER-Hoxb8 compared to BMD macrophages after intracranial transplantation in *Csf1r*$^{-/-}$ hosts. (A) Schematic for in vivo *Csf1r*$^{-/-}$ transplant experiments **(B)** Rendered tile stitches of *Csf1r*$^{-/-}$ brains after intracranial injection of GFP+ bone marrow (left) or ER-Hoxb8 (right) progenitor cells **(C)** Percent of total brain area tiled by donor cells; n = five to seven biological replicates per group; each dot = one biological replicate (average area across three matched sagittal sections) **(D)** Immunostaining of cortical brain region 12-16 days post-intracranial injection (red = IBA1, green = endogenous GFP, blue = DAPI; scale bar = 100um; inset scale bar = 5um) **(E)** Cortical density calculations (cells per mm^2) between groups; n = five to seven biological replicates per group; each dot = one biological replicate (average density across three regions of interest across three matched sagittal sections). All p-values calculated via one-way ANOVA with multiple comparisons; ns = not significant or p >= 0.05, ****p < 0.0001

Panel A created with BioRender.com/j85e198

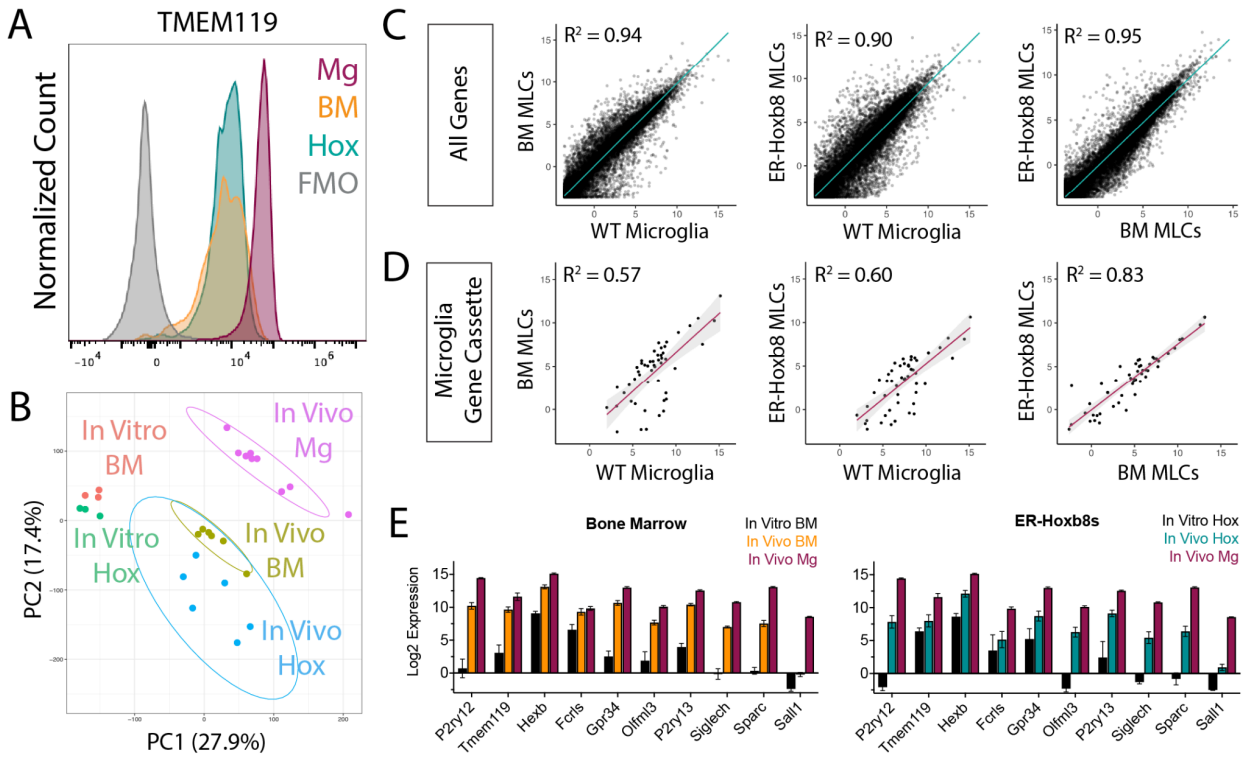

Figure 3: ER-Hoxb8 macrophages become microglia-like cells (MLCs) after engraftment in the *Csf1r*$^{-/-}$ brain. (A) Histogram of TMEM119 surface staining by flow cytometry (pre-gated on live, singlet, leukocyte, CD45+/CD11B+) for brain-engrafted cells 14 days post-intracerebral transplantation; Mg = WT Microglia, BM = BMD MLCs, Hox = ER-Hoxb8 MLCs (**B)** PCA plot comparing in vitro macrophages from Figure 1 with in vivo macrophages; Mg = WT Microglia, BM = BMD MLCs, Hox = ER-Hoxb8 MLCs (**C)** Whole transcriptome comparison between WT microglia, BMD, and ER-Hoxb8 macrophages in vivo, depicting best fit line and the coefficient of determination (**D)** Comparison of microglia signature genes (Cronk, et al. *JEM* (2018)) depicting best fit line and coefficient of determination **(E)** In vitro and in vivo Log2 CPM gene expression of ten canonical microglia/myeloid genes for bone marrow (left) and ER-Hoxb8s (right) as compared to unmanipulated in vivo microglia

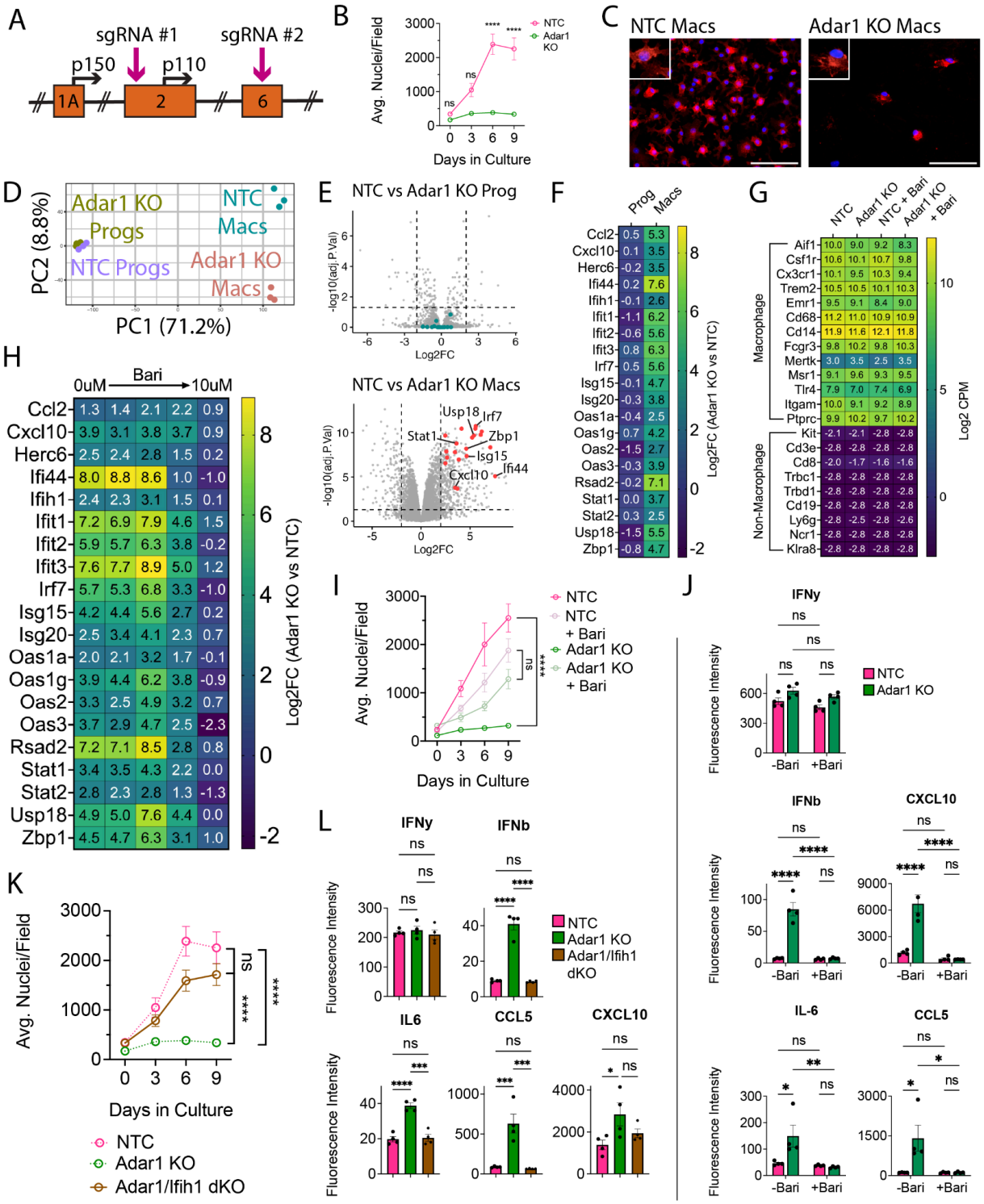
A
sgRNA #1
sgRNA #2
p150
p110
1A
2
6
B
Avg. Nuclei/Field
Days in Culture
NTC
Adar1 KO
C
NTC Macs
Adar1 KO Macs
D
Adar1 KO Progs
NTC Macs
NTC Progs
Adar1 KO Macs
PC2 (8.8%)
PC1 (71.2%)
E
NTC vs Adar1 KO Prog
NTC vs Adar1 KO Macs
-log10(adj.P.Val)
Log2FC
Usp18
Irf7
Stat1
Zbp1
Isg15
Ifi44
Cxcl10
F
Prog
Macs
Log2FC (Adar1 KO vs NTC)
G
NTC
Adar1 KO
NTC + Bari
Adar1 KO + Bari
Macrophage
Non-Macrophage
Log2 CPM
H
0uM
Bari
10uM
Log2FC (Adar1 KO vs NTC)
I
NTC
NTC + Bari
Adar1 KO
Adar1 KO + Bari
Avg. Nuclei/Field
Days in Culture
J
IFNy
IFNb
CXCL10
IL-6
CCL5
Fluorescence Intensity
-Bari
+Bari
K
Avg. Nuclei/Field
Days in Culture
NTC
Adar1 KO
Adar1/Ifih1 dKO
L
IFNy
IFNb
IL6
CCL5
CXCL10
Fluorescence Intensity
Adar1/Ifih1 dKO

Figure 4: *Adar1* mutation prevents macrophage-lineage cell expansion and causes interferon induction, rescued by JAKi or *Ifih1* mutation. (A) Schematic of ADAR1 locus, depicting exons, alternative start sites for p150 and p110 isoforms, and sgRNA targets **(B)** ER-Hoxb8 cell counts over differentiation time course **(C)** Immunostaining of in vitro, eight-day differentiated macrophages comparing control (NTC) and *Adar1* guide-transduced macrophages (red = CD11B, blue = DAPI; scale bar = 100um) **(D)** PCA plot of progenitors and macrophages in vitro **(E)** Volcano plots showing differentially expressed genes between *Adar1* KO and NTC progenitors and macrophages (CPM > 1, Log2FC >= 2, FDR < 0.05) **(F)** Heatmap showing the Log2FC (*Adar1* KO values over NTC values) for relevant interferon-stimulated genes **(G)** Heatmap showing Log2 CPM of canonical macrophage (top) and non-macrophage (bottom) immune cell genes **(H)** Heatmap showing Log2FC (*Adar1* KO over NTC expression) for interferon-stimulated genes in macrophages treated with baricitinib **(I)** ER-Hoxb8 cell counts over differentiation time course, comparing the effect of baricitinib on *Adar* KO and NTC lines (dosages = 0uM, 0.00064uM, 0.16uM, 0.4uM, and 10uM); statistics calculated at the 9 day time point **(J)** Interferon, cytokine and chemokine production after treatment with baricitinib via cytokine bead array **(K)** ER-Hoxb8 cell counts over differentiation time course, comparing NTC, *Adar1* KO, and *Adar/Ifih1* double KO (dKO) lines - dotted NTC and *Adar1* KO lines are equivalent to those shown in panel (B) **(L)** Interferon, cytokine and chemokine production via cytokine bead array, comparing NTC, *Adar* KO, and *Adar/Ifih1* dKO lines. All p-values calculated via one-way (L) or two-way (B, I, J, K) ANOVA with multiple comparisons; ns = not significant or p >= 0.05, *p < 0.05, **p < 0.01, ***p < 0.001, ****p < 0.0001

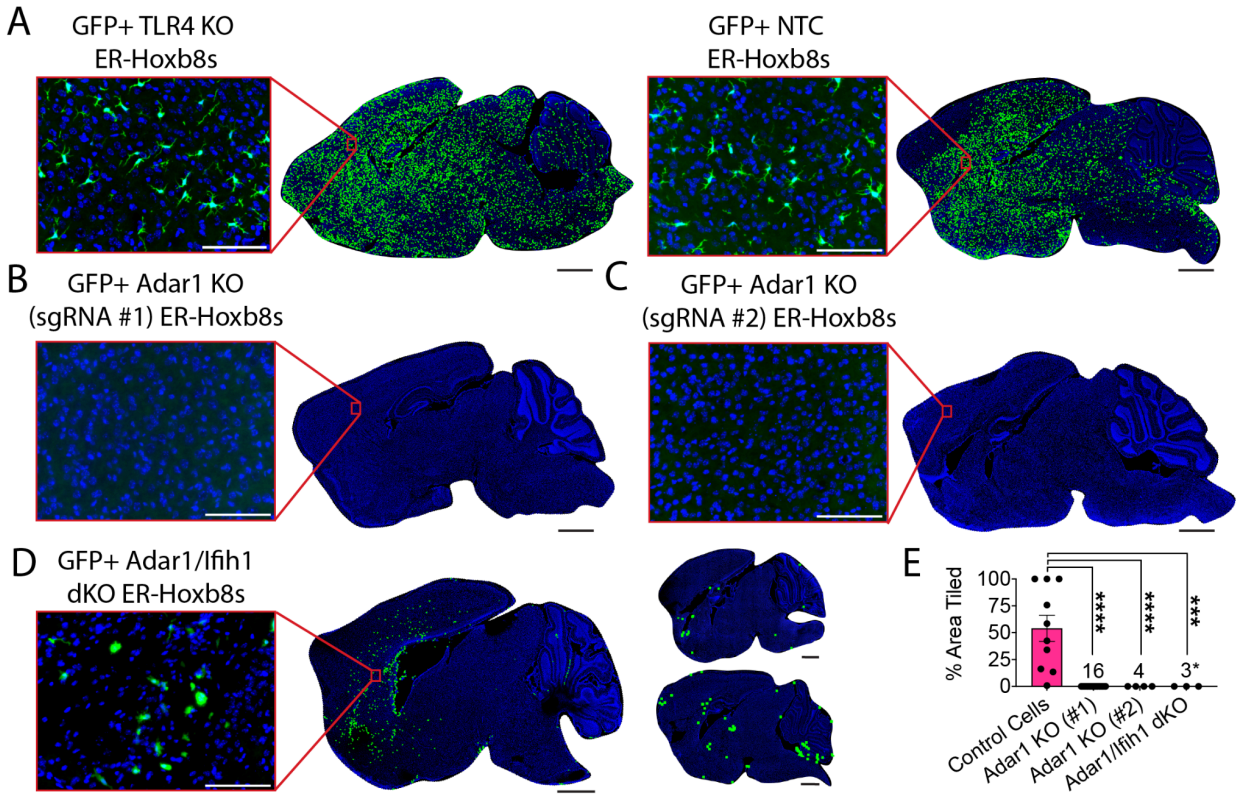

Figure 5: *Adar1* mutation prevents ER-Hoxb8 engraftment in the *Csf1r*$^{-/-}$ mouse, partially rescued by *Ifih1* deletion. (A) Representative rendering of donor cell engraftment (scale bar = 1000um) with inset microscopy of GFP+ donor cell engraftment (green = endogenous GFP, blue = DAPI; scale bar = 100um) for control cells (TLR4 KO and NTC) harvested 7-15 days post-injection (dpi), **(B)** *Adar1* KO (sgRNA #1) cells (harvest details in (E)), **(C)** *Adar1* KO (sgRNA #2) cells harvested 9-12dpi, and **(D)** *Adar1*/*Ifih1* double KO (dKO) cells harvested 10-15dpi (rendered dots in two right brains enlarged 5x for visualization) **(E)** Percent of total brain area tiled with cells between groups (numbers denote "n" per group); *Adar1* KO (#1) cells include pooled data (brains injected with 300k cells/hemisphere, harvested at 10-15 days post-injection (dpi; n = 3); brains injected with 300k cells/hemisphere, harvested at 4-8dpi (n=8); brains injected with 50k cells/hemisphere, harvested at 13dpi (n = 4); and brains injected with 100k cells/hemisphere pre-treated with 0.5uM Baricitinib, mice treated daily with 1mg/kg Baricitinib, harvested at 5dpi (n = 1)); asterisk indicates samples where engraftment is present but does not meet criteria for tiled brain area, as exemplified in (D); p-values calculated via one-way ANOVA with multiple comparisons; ns = not significant or p >= 0.05, ***p < 0.001, ****p < 0.0001

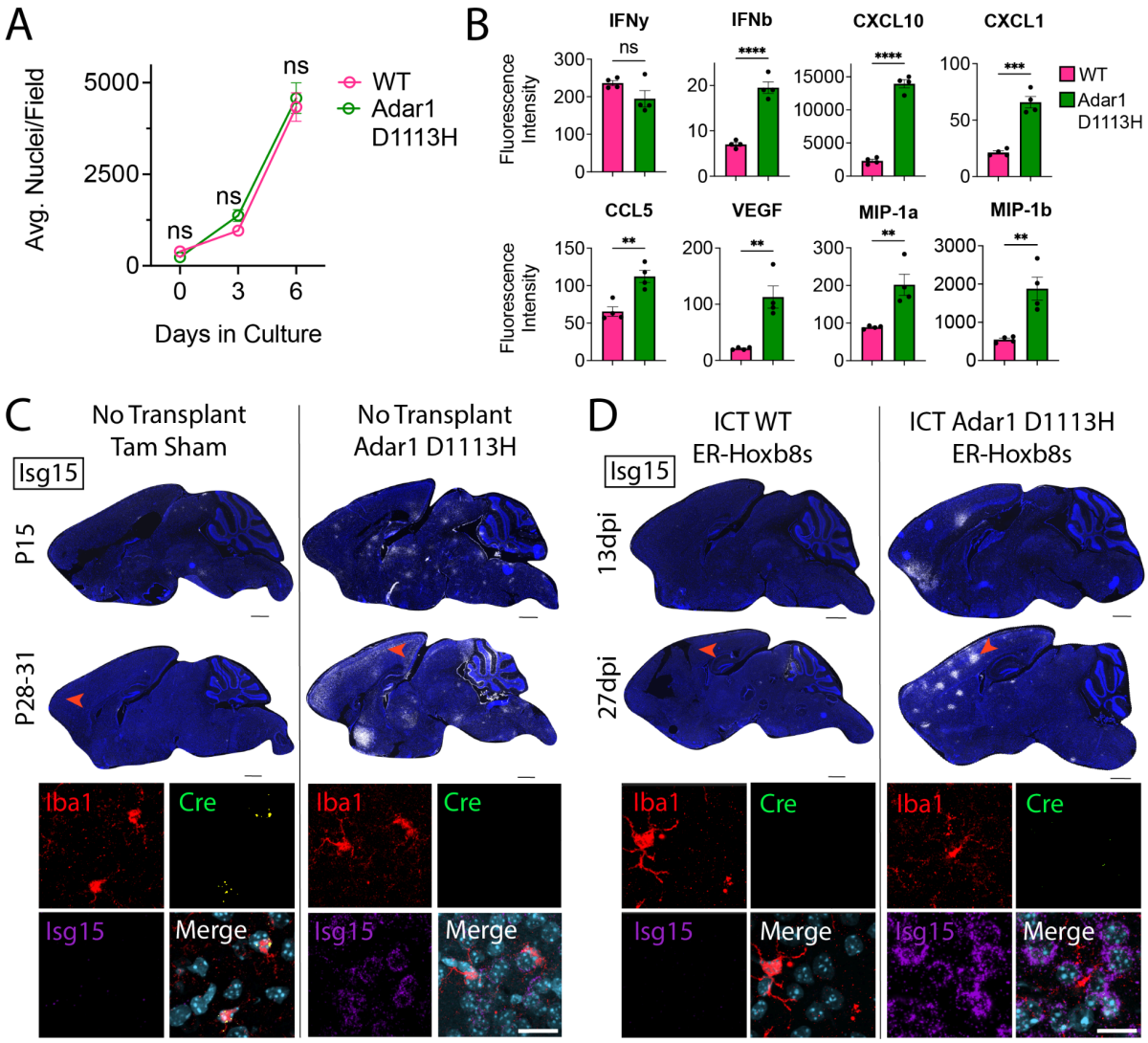

Figure 6: *Adar1* D1113H mutant ER-Hoxb8 macrophages persistently drive brain ISG expression. (A) In vitro ER-Hoxb8 cell counts over time (p-values calculated via two-way ANOVA with multiple comparisons) **(B)** Multiplex bead array data for interferons, cytokines, and chemokines produced via ER-Hoxb8 macrophages (p-values calculated via independent two-sample t-test) **(C)** Sagittal sections of non-transplanted (tamoxifen (tam) sham control) *Cx3cr1*^{CreERT}; *Csf1r*$^{fl/fl}$ brains (left) and *Adar1* D1113H mutant brains (right) at age P15 and P28-31; nuclei (blue, DAPI), *Isg15* (white via RNA in situ hybridization (ISH)); scale bar = 1000um; red arrow depicts location of corresponding closeup images below, showing IBA1 (red, protein stain), *Cre* (green, ISH), *Isg15* (purple, ISH), and nuclei (teal, DAPI); scale bar = 20um; see Supplemental Figure 7A for further corresponding closeup images **(D)** Sagittal sections of *Cx3cr1*^{CreERT}; *Csf1r*$^{fl/fl}$ brains intracranially transplanted with WT ER-Hoxb8s (left) and *Adar1* D1113H ER-Hoxb8s (right) at 13 and 27 days post-injection (dpi); nuclei (blue,

DAPI), *Isg15* (white, ISH); scale bar = 1000um; red arrow depicts location of corresponding closeup images below, showing IBA1 (red, protein stain), *Cre* (green, ISH), *Isg15* (purple, ISH), and nuclei (teal, DAPI); scale bar = 20um; see Supplemental Figure 7A for further corresponding closeup images. All p-values characterized by: ns = not significant or $p >= 0.05$, *$p < 0.05$, **$p < 0.01$, ***$p < 0.001$, ****$p < 0.0001$

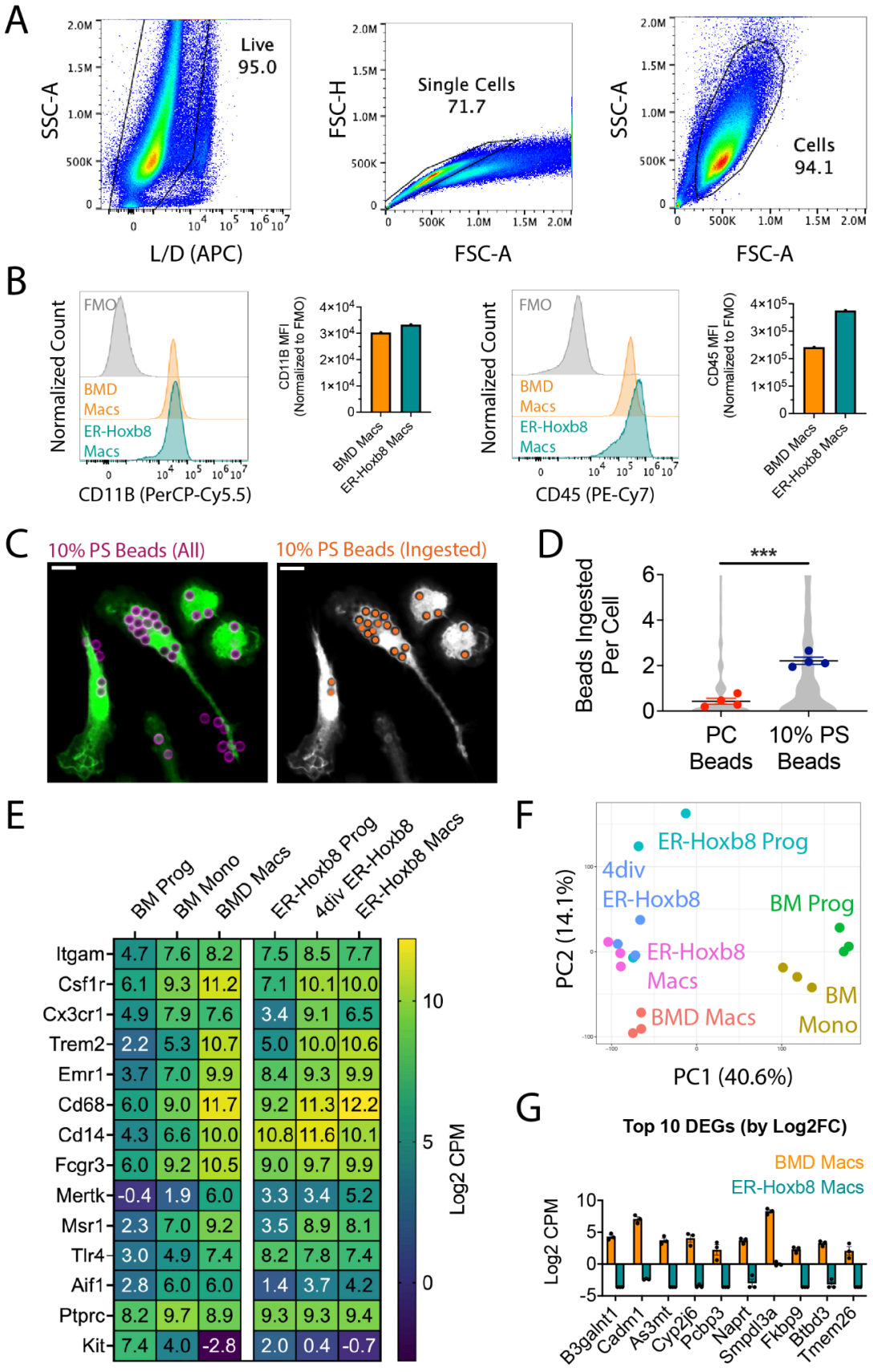
A
Live
95.0
SSC-A
L/D (APC)
Single Cells
71.7
FSC-H
FSC-A
Cells
94.1
SSC-A
FSC-A
B
FMO
BMD
Macs
ER-Hoxb8
Macs
Normalized Count
CD11B (PerCP-Cy5.5)
CD11B MFI
(Normalized to FMO)
BMD Macs
ER-Hoxb8 Macs
CD45 (PE-Cy7)
CD45 MFI
(Normalized to FMO)
C
10% PS Beads (All)
10% PS Beads (Ingested)
D
***
Beads Ingested
Per Cell
PC
Beads
10% PS
Beads
E
BM Prog
BM Mono
BMD Macs
ER-Hoxb8 Prog
4div ER-Hoxb8
ER-Hoxb8 Macs
Itgam 4.7 7.6 8.2 7.5 8.5 7.7
Csf1r 6.1 9.3 11.2 7.1 10.1 10.0
Cx3cr1 4.9 7.9 7.6 3.4 9.1 6.5
Trem2 2.2 5.3 10.7 5.0 10.0 10.6
Emr1 3.7 7.0 9.9 8.4 9.3 9.9
Cd68 6.0 9.0 11.7 9.2 11.3 12.2
Cd14 4.3 6.6 10.0 10.8 11.6 10.1
Fcgr3 6.0 9.2 10.5 9.0 9.7 9.9
Mertk -0.4 1.9 6.0 3.3 3.4 5.2
Msr1 2.3 7.0 9.2 3.5 8.9 8.1
Tlr4 3.0 4.9 7.4 8.2 7.8 7.4
Aif1 2.8 6.0 6.0 1.4 3.7 4.2
Ptprc 8.2 9.7 8.9 9.3 9.3 9.4
Kit 7.4 4.0 -2.8 2.0 0.4 -0.7
Log2 CPM
F
ER-Hoxb8 Prog
4div
ER-Hoxb8
BM Prog
ER-Hoxb8
Macs
BM
Mono
BMD Macs
PC2 (14.1%)
PC1 (40.6%)
G
Top 10 DEGs (by Log2FC)
BMD Macs
ER-Hoxb8 Macs
Log2 CPM
B3galnt1
Cadm1
As3mt
Cyp2j6
Pcbp3
Naprt
Smpdl3a
Fkbp9
Btbd3
Tmem26

Supplemental Figure 1: Extended validation and comparison of ER-Hoxb8 to BMD macrophages in vitro, relating to Figure 1. (A) Gating strategy for Figure 1C **(B)** Flow cytometry histograms and median fluorescence intensity (MFI) of CD11B (left) and CD45 (right), relating to Figure 1C **(C)** Merged image of ER-Hoxb8 macrophages (green) and synthetic apoptotic cell corpse mimics (10% PS beads, purple) imaged after fixation and staining (orange denotes beads counted as ingested) **(D)** Quantification of phagocytosis of synthetic apoptotic cell corpse mimics (10% PS beads) as compared to synthetic live cell mimic controls (PC beads); p-value calculated via nested t-test for n=4 replicates per group, with overall distribution (81-100 cells per replicate) shown in gray; ***$p < 0.001$ **(E)** Heatmap showing Log2 CPM gene expression levels of macrophage genes across groups; progenitor and macrophage groups are as represented in Figure 1A, BM Mono = monocytes isolated from BM, 4div ER-Hoxb8 = ER-Hoxb8s collected after four days of in vitro differentiation **(F)** PCA plot combining bulk RNA sequencing data amongst all groups **(G)** Log2 CPM values of top 10 differentially expressed genes by Log2FC (CPM > 1, Log2FC >= 2, FDR < 0.05)

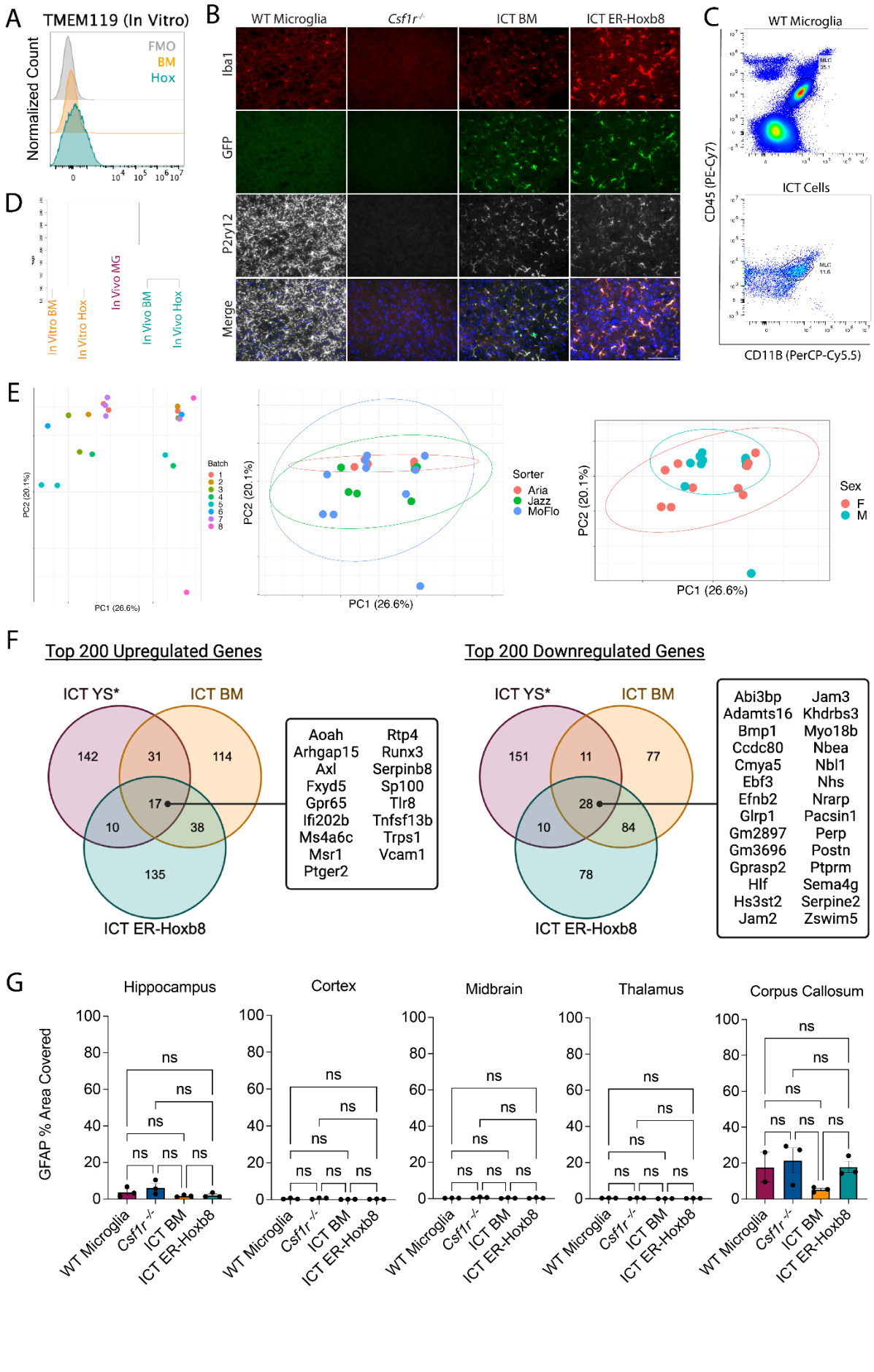
A
TMEM119 (In Vitro)
Normalized Count
FMO
BM
Hox
B
WT Microglia
Csf1r-/-
ICT BM
ICT ER-Hoxb8
Iba1
GFP
P2ry12
Merge
C
WT Microglia
ICT Cells
CD45 (PE-Cy7)
CD11B (PerCP-Cy5.5)
D
In Vitro BM
In Vitro Hox
In Vivo MG
In Vivo BM
In Vivo Hox
E
Batch
PC1 (26.6%)
PC2 (20.1%)
Sorter
Aria
Jazz
MoFlo
Sex
F
M
F
Top 200 Upregulated Genes
ICT YS*
ICT BM
ICT ER-Hoxb8
142
31
114
17
10
38
135
Aoah
Arhgap15
Axl
Fxyd5
Gpr65
Ifi202b
Ms4a6c
Msr1
Ptger2
Rtp4
Runx3
Serpinb8
Sp100
Tlr8
Tnfsf13b
Trps1
Vcam1
Top 200 Downregulated Genes
151
11
77
28
10
84
78
Abi3bp
Adamts16
Bmp1
Ccdc80
Cmya5
Ebf3
Efnb2
Glrp1
Gm2897
Gm3696
Gprasp2
Hlf
Hs3st2
Jam2
Jam3
Khdrbs3
Myo18b
Nbea
Nbl1
Nhs
Nrarp
Pacsin1
Perp
Postn
Ptprm
Sema4g
Serpine2
Zswim5
G
Hippocampus
Cortex
Midbrain
Thalamus
Corpus Callosum
GFAP % Area Covered
ns
WT Microglia
Csf1r-/-
ICT BM
ICT ER-Hoxb8

Supplemental Figure 2: Extended comparison of ER-Hoxb8 and BMD macrophages after intracranial transplantation in *Csf1r*$^{-/-}$ hosts, relating to Figure 3. (A) Histogram of TMEM119 surface staining by flow cytometry (pre-gated on live, singlet, leukocyte, CD45+/CD11b+) for seven-day differentiated in vitro BMD and ER-Hoxb8 macrophages **(B)** Immunostaining of cortical brain region 12-16 days post-intracranial injection (red = IBA1, green = endogenous GFP, white = P2RY12; blue = DAPI; scale bar = 100um) **(C)** Gating strategy for in vivo TMEM119 histogram shown in Figure 3A (pre-gated on live, singlet, leukocyte, GFP) of WT microglia and intracranially transplanted (ICT) cells (BM or ER-Hoxb8s) **(D)** Unsupervised hierarchical cluster dendrogram, related to Figure 3B (distance method = euclidean; cluster method = complete) **(E)** Comparison of "batch" by PCA plots for harvest days (left), sorter used (middle), and host mouse sex (right) **(F)** Venn diagrams comparing the top 200 up and downregulated genes, as compared to unmanipulated in vivo microglia; asterisk denotes data derived from previously published dataset (Bennett et al., 2018); genes were rank-ordered by absolute expression value, with only the top 1000 being considered for comparison, sorted by Log2FC > 2, FDR < 0.5, and ordered by Log2FC values **(G)** Quantification of GFAP percent area covered; n = 3 biological replicates per group; each dot = one biological replicate (average area across three matched sagittal sections); p-values calculated via one-way ANOVA with multiple comparisons; ns = not significant or p >= 0.05

Panel F created with BioRender.com/2k8tqf3

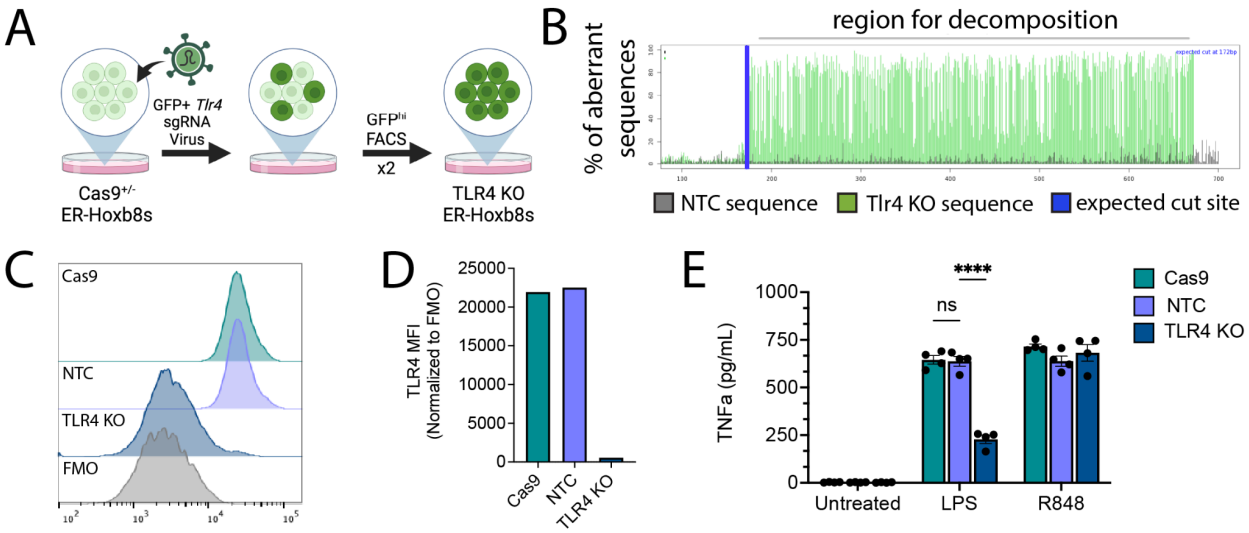

Supplemental Figure 3: CRISPR-Cas9 editing of ER-Hoxb8 progenitors, relating to Figures 4 and 5. (A) Schematic for *Tlr4* knockout using Cas9$^{+/-}$ ER-Hoxb8s and sgRNA viral transduction **(B)** Post-editing trace decomposition charts (via TIDE Analysis) for *Tlr4* KO macrophages **(C)** Histogram of TLR4 surface staining by flow cytometry (pre-gated on live, singlet, leukocyte) for eight day-differentiated in vitro BMD and ER-Hoxb8 macrophages **(D)** TLR4 median fluorescence intensity (MFI) normalized to FMO levels using flow cytometry data shown in C **(E)** TNF*a* production, comparing control, LPS, and R848 treated samples (eight-day differentiation, 9.5h LPS or R848, 100ng/mL, n = four replicates per condition); p-values calculated via two-way ANOVA with multiple comparisons; ns = not significant or p >= 0.05, ****p < 0.0001

Panel A created with BioRender.com/q68t656

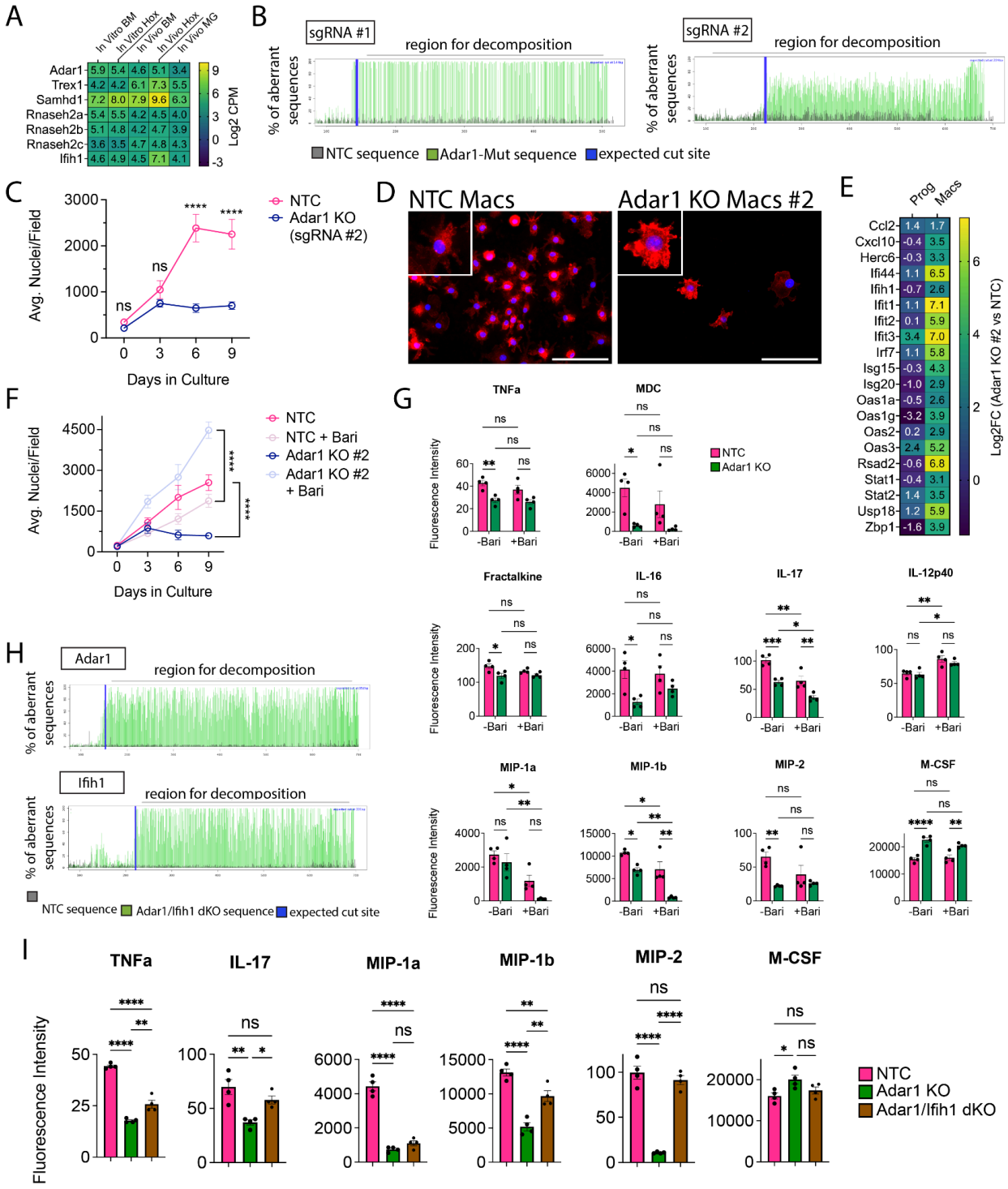
A
In Vitro BM
In Vitro Hox
In Vivo BM
In Vivo Hox
In Vivo MG
Adar1 5.9 5.4 4.6 5.1 3.4
Trex1 4.2 4.2 6.1 7.3 5.5
Samhd1 7.2 8.0 7.9 9.6 6.3
Rnaseh2a 5.4 5.5 4.2 4.5 4.0
Rnaseh2b 5.1 4.8 4.2 4.7 3.9
Rnaseh2c 3.6 3.5 4.7 4.8 4.3
Ifih1 4.6 4.9 4.5 7.1 4.1
Log2 CPM
B
sgRNA #1
region for decomposition
% of aberrant sequences
sgRNA #2
region for decomposition
% of aberrant sequences
NTC sequence
Adar1-Mut sequence
expected cut site
C
Avg. Nuclei/Field
Days in Culture
NTC
Adar1 KO (sgRNA #2)
ns
****
D
NTC Macs
Adar1 KO Macs #2
E
Prog
Macs
Log2FC (Adar1 KO #2 vs NTC)
F
Avg. Nuclei/Field
Days in Culture
NTC
NTC + Bari
Adar1 KO #2
Adar1 KO #2 + Bari
G
TNFa
MDC
Fractalkine
IL-16
IL-17
IL-12p40
MIP-1a
MIP-1b
MIP-2
M-CSF
Fluorescence Intensity
-Bari
+Bari
NTC
Adar1 KO
H
Adar1
region for decomposition
% of aberrant sequences
Ifih1
region for decomposition
% of aberrant sequences
NTC sequence
Adar1/Ifih1 dKO sequence
expected cut site
I
TNFa
IL-17
MIP-1a
MIP-1b
MIP-2
M-CSF
Fluorescence Intensity
NTC
Adar1 KO
Adar1/Ifih1 dKO

Supplemental Figure 4: Evidence for gene knockout (KO), *Adar1* sgRNA #2 results, and extended bead array data, relating to Figure 4. (A) Heatmap of Log2 CPM expression of seven causal AGS genes in BMD and ER-Hoxb8 macrophages **(B)** Post-editing trace decomposition charts (via TIDE Analysis) for *Adar1* KO cells targeted with two distinct guides **(C)** ER-Hoxb8 cell counts over time **(D)** Immunostaining of in vitro, eight-day differentiated macrophages comparing control (NTC) and *Adar1* sgRNA #2-transduced macrophages (red = CD11B, blue = DAPI; scale bar = 100um) **(E)** Heatmap showing the Log2FC (*Adar1* KO values over NTC values) for relevant interferon-stimulated genes for both progenitors and macrophages at baseline **(F)** Validation of in vitro ER-Hoxb8 cell counts with vehicle or 10uM baricitinib treatment using *Adar1* sgRNA #2; statistics calculated at the 9 day time point **(G)** Interferon, cytokine and chemokine production for ER-Hoxb8 macrophages grown with or without baricitinib, via cytokine bead array **(H)** Trace decomposition charts (via TIDE Analysis) for *Adar1*/*Ifih1* double KO (dKO) cell lines **(I)** Interferon, cytokine and chemokine production for ER-Hoxb8 macrophages with or without subsequent *Ifih1* KO. All p-values calculated via one-way (I) or two-way (C, F, G) ANOVA with multiple comparisons; ns = not significant or $p >= 0.05$, *$p < 0.05$, **$p < 0.01$, ***$p < 0.001$, ****$p < 0.0001$

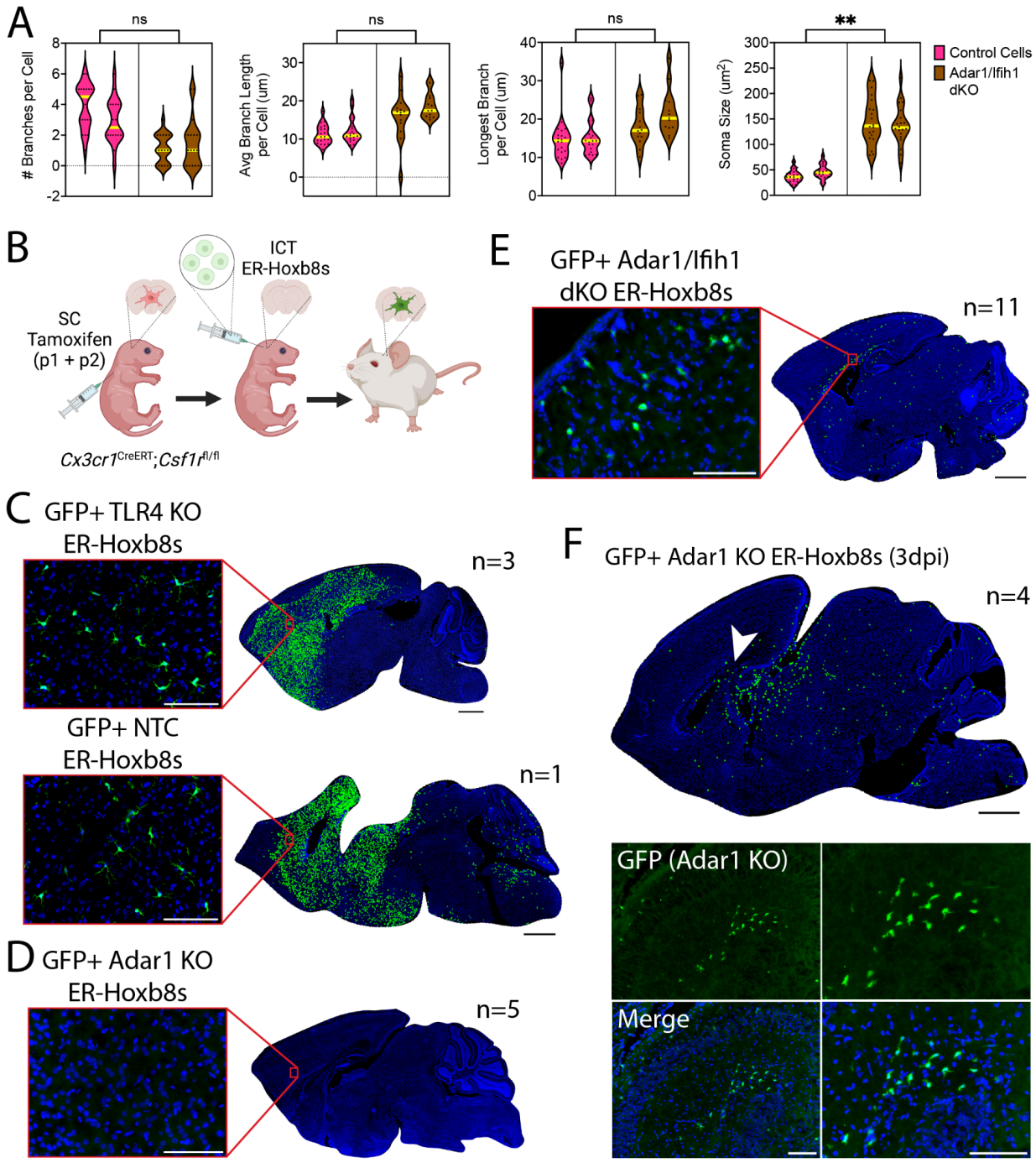

Supplemental Figure 5: Concurrent *Adar1*, *Ifih1* mutation morphology, plus engraftment in the *Cx3cr1*^{CreERT}; *Csf1r*$^{fl/fl}$ mouse, relating to Figure 5. (A) Violin plot of all analyzed cortical ER-Hoxb8 cells (n=20) per animal (n=2), with yellow line denoting the median, for number of primary branches, average length of branches, longest branch length, and soma size; p-value calculated via nested t-test for n=2 animals per group; ns = not significant or p >= 0.05, **p < 0.005 **(B)** Schematic for in

vivo *Cx3cr1*^{CreERT}; *Csf1r*$^{fl/fl}$ transplant experiments **(C)** Representative rendering of donor cell engraftment (scale bar = 1000um) with inset microscopy of GFP+ donor cell engraftment (green = endogenous GFP, blue = DAPI; scale bar = 100um) for control cells (TLR4 KO, NTC) harvested 15 days post-injection, **(D)** *Adar1* KO cells harvested seven days post-injection, **(E)** *Adar1*/*Ifih1* double KO (dKO) cells harvested 13-15 days post-injection, and **(F)** *Adar1* KO cells harvested three days post-injection

Panel B created with BioRender.com/n75g136

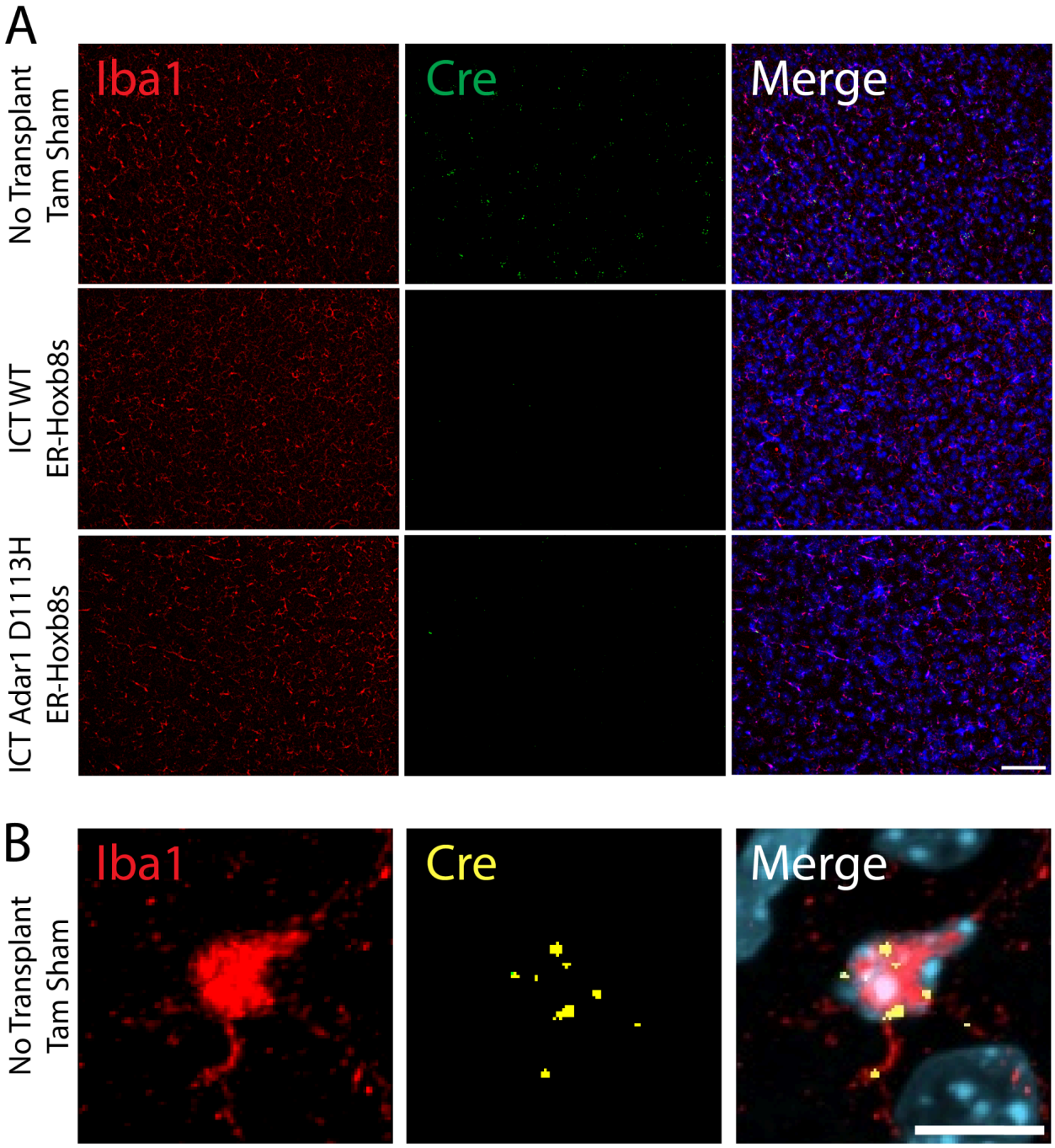

Supplemental Figure 6: Evidence for *Cre* expression, relating to Figure 6. (A) Dual immunostaining/RNA in situ hybridization (ISH) showing IBA1 (red, protein stain), *Cre* (green, ISH), and nuclei (blue, DAPI); scale bar = 100um **(B)** magnified image of a repopulated microglia from the non-transplanted (tam sham control) *Cx3cr1*^{CreERT}; *Csf1r*$^{fl/fl}$ brain shown in (A); scale bar = 10um

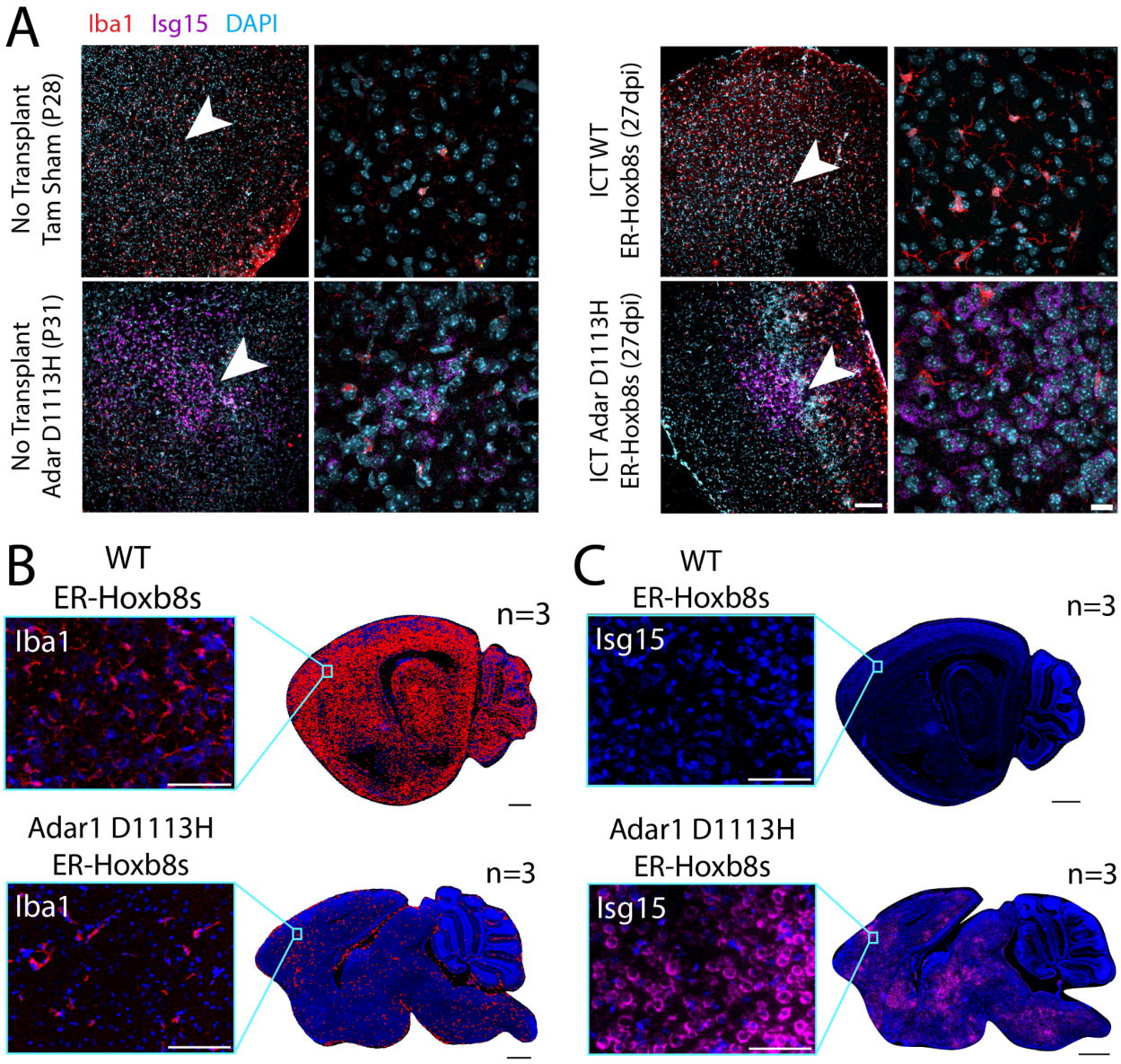

Supplemental Figure 7: Extended *Isg15* RNA in situ hybridization (ISH), relating to Figure 6. (A) Dual immunostaining/RNA ISH showing IBA1 (red, protein stain), *Isg15* (purple, ISH), and nuclei (teal, DAPI); scale bar = 100um; white arrow depicts location of corresponding close up image; scale bar = 20um **(B)** Representative rendering of donor cell engraftment in the *Csf1r*$^{-/-}$ brain (scale bar = 1000um) with inset microscopy of IBA1+ donor cell engraftment (red = IBA1, blue = DAPI; scale bar = 100um) for FVB Osb-GFP WT ER-Hoxb8s and *Adar1* D1113H mutant ER-Hoxb8s harvested 13-14 days post-injection **(C)** Dual immunostaining/RNA ISH for samples shown in (B); tile scale bar = 1000um; inset = *Isg15* (pink, ISH), nuclei (blue, DAPI); scale bar = 100um